COMMUNICATION

Inducing Molecular Reactions by Selective Vibrational Excitation of a Remote Antenna with Near-Infrared Light

Received 00th January 20xx,
Accepted 00th January 20xx

DOI: 10.1039/x0xx00000x

Cláudio M. Nunes,* Nelson A. M. Pereira, Luís P. Viegas, Teresa M. V. D. Pinho e Melo, and Rui Fausto

We demonstrate here that selective vibrational excitation of a moiety, remotely attached in relation to the molecular reaction site, might offer a generalized strategy for inducing bond-breaking/bond-forming reactions with exquisite precision. As a proof-of-principle, the electrocyclic ring-expansion of a benzazirine to a ketenimine was induced, in a cryogenic matrix, by near-IR light tuned at the overtone stretching frequency of its OH remote antenna. This accomplishment paves the way for harnessing IR vibrational excitation as a tool to guide a variety of molecular structure manipulations in unprecedent highly-selective fashion.

Since the invention of lasers in the 1960s, chemists have dreamt of using infrared (IR) laser radiation to manipulate matter in an unprecedented selective way.[1–4] The possibility of selectively manipulate a chosen molecular species in a complex mixture, including the manipulation of a specific conformation existing in a particular environment, has been demonstrated using vibrational excitation in conjugation with the matrix isolation technique.[5,6] In this context, narrowband IR-light is applied to selectively deposit energy in a vibrational state of a particular molecular system. If subsequent energy dissipation by intramolecular vibrational redistribution is partially channeled to a reaction coordinate, a transformation might be induced with a potential exquisite precision.[7,8]

In the last twenty years, this methodology has been employed to manipulate molecular conformations of different types of organic compounds, such as carboxylic acids,[9,10] alcohols,[11,12] amino acids,[13,14] and nucleic acid derivatives.[15] Most of the reported cases comprise the vibrational excitation of an OH moiety (typically at its first stretching overtone) and conformational isomerization at the same OH moiety or at an adjacent CC bond. A significant development was made in 2015, when the interconversion between two conformers was shown to be possible by selective vibrational excitation of a moiety (antenna), remotely located from the conformational isomerization coordinate (Scheme 1).[16,17]

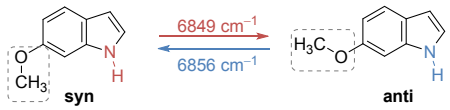

Scheme 1. Conformational changes in 6-methoxyindole (Xe, 30 K) induced by vibrational excitation of the remote NH antenna at its first stretching overtone.[16]

In 2020, we demonstrated that, besides conformational isomerizations, bond-breaking/bond-forming reactions can also be induced by IR vibrational excitation under matrix isolation conditions.[18,19] In that breakthrough investigation, the bidirectional tautomerization (thione-enol ↔ thiol-keto) of thiotropolone was triggered by IR-irradiation of the corresponding reactant tautomeric form. A few other separate studies[20] have also reported examples of bond-breaking or bond-breaking/bond-forming reactions promoted by vibrational excitation of organic molecules in gas-phase at low-pressure[21–24] and in solution.[25–27] However, the use of IR vibrational excitation to induce transformations of organic molecules still remains vastly unexplored and hindered by the lack of a functioning approach.

Herein, we set the stage for a generalized approach aiming to induce bond-breaking/bond-forming reactions in organic molecules by IR vibrational excitation. Our envisioned strategy consists of using a vibrational antenna remotely located from the reaction center of the target molecule, following the principle previously established to control conformational changes. As a proof-of-principle of such approach, we demonstrate here that selective vibrational excitation of the OH moiety of benzazirine **3** successfully triggers its electrocyclic ring-expansion to cyclic ketenimine **4** (Scheme 2).

Benzazirines are highly reactive intermediates, with very low-energy barriers for ring-opening to phenylnitrenes and ring-expansion to cyclic ketenimines.[28–30] Therefore, they are particularly suitable species to be activated by IR vibrational excitation. The presence of two *ortho* fluorine atoms in a benzazirine is known to increase the reactions barriers enough to make the system stable against tunneling and allow its capture under cryogenic conditions.[31,32] In the present study, the introduction of a *para* OH substituent was conceived to act

University of Coimbra, CQC, Department of Chemistry, 3004-535 Coimbra, Portugal
Email: cmnunes@qui.uc.pt
† Electronic Supplementary Information (ESI) available: For experimental and computational methods, additional figures and tables, and computational data see DOI: 10.1039/x0xx00000x

as a remote vibrational antenna. Thus, 4-hydroxy-2,6-difluoro-2*H*-benzazirine **3** resulted as an idealized target for the realization of this proof-of-principle study.

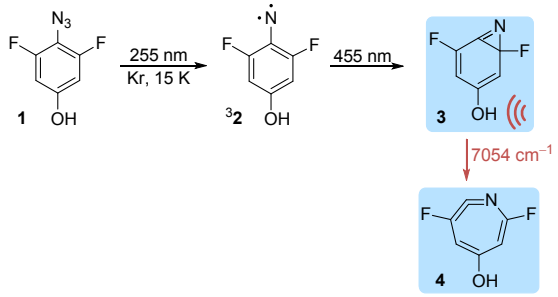

Scheme 2. Summary of the experimental results concerning the ring-expansion of benzazirine **3** to cyclic ketenimine **4** (Kr, 15 K) induced by vibrational excitation of the remote OH antenna at its first stretching overtone (7054 cm^{-1}).

The precursor, 2,6-difluoro-4-hydroxyphenylazide **1**, was synthesized as described in detail in the Supporting Information (SI). Cryogenic matrices of **1** were prepared by sublimating the sample at room temperature and co-deposited it with a large excess of Kr onto a CsI window at 15 K (Fig. S1). The UV-irradiation (λ = 255 nm) of matrix-isolated **1** leads to triplet 2,6-difluoro-4-hydroxyphenylnitrene ^{3}**2**. The bands that appear in the IR spectrum after irradiation of **1** are well reproduced by the B3LYP/6-311+G(2d,p) computed IR spectrum of ^{3}**2** (Fig. 1a,b). Particularly characteristic are the most intense IR bands observed at 1602/1599, 1468, 1220, 1139/1137 and 1018 cm^{-1}, which nicely match the most intense computed IR bands of ^{3}**2** at 1598 [ν(CC)], 1453 [ν(CC)], 1206 [δ(CH)], 1134 [ν(CO)] and 1007 [$\nu(CF)_{as}$] cm^{-1}. A detailed assignment of the IR spectrum of nitrene ^{3}**2** is provided in Table S1.

Subsequent visible-light irradiation of nitrene ^{3}**2**, at the low-energy edge of its first absorption band (λ = 445 nm),[33] was found to produce mainly *syn*-2,6-difluoro-4-hydroxy-2*H*-benzazirine **3s**. With the exception of a few minor bands of an unidentified product,[34] the bands that emerge in the IR spectrum after consumption of ^{3}**2** have a good correspondence with the B3LYP/6-311+G(2d,p) computed IR spectrum of **3s** (Fig. 1c,d). Most representative are the IR bands observed at 1620, 1316, 1201, 1144, 1118/1111 and 934/932 cm^{-1}, which are well reproduced by the high intensity computed IR bands of **3s** at 1614 [ν(C=C)], 1308 [δ(CH), ν(C-C)], 1185 [ν(CF)], 1134 [ν(CO)], 1095 [ν(CF)] and 918 [ν(C-C)] cm^{-1}. The characteristic absorption due to the ν(C=N) mode of **3s** is identified at 1685 cm^{-1}, near the absorption frequency previously reported for the 2,6-difluoro-2*H*-benzazirine analog (1679 cm^{-1}, Ar matrix at 10 K).[32] The presence of the *anti*-OH conformer **3a** was excluded, as some of its distinctive computed IR bands have no correspondence in the experimental IR spectrum (Fig. S2). A comprehensive assignment of the IR spectrum of benzazirine **3s** is given in Table S2, supported also by additional data addressed in the next section. According to our expectation, **3s** was found to be stable in a Kr matrix at 15 K (no trace of any transformation was detected after waiting 24 h).

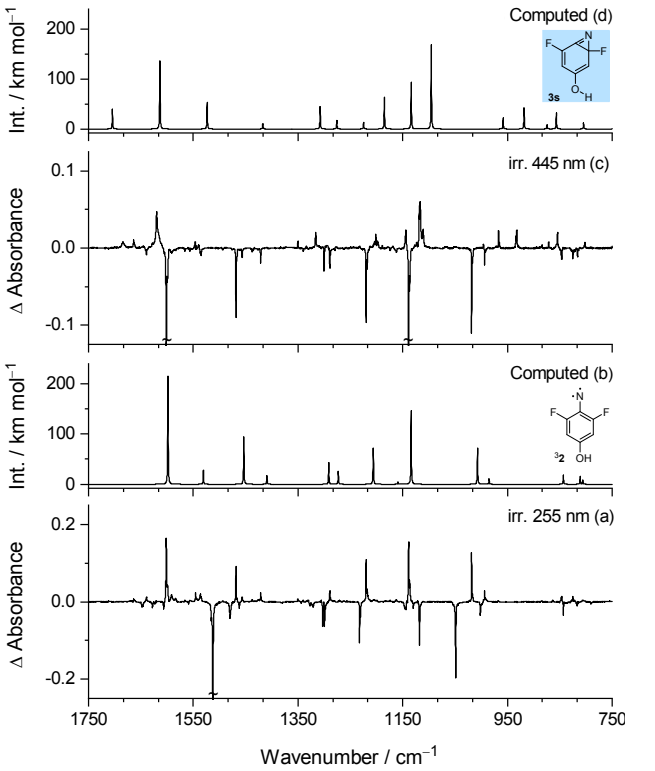

Fig. 1. Experimental difference IR spectrum showing changes that result from: (a) irradiation of azide **1** at 255 nm (8 min, 30 mW, Kr matrix at 15 K); (c) irradiation of triplet nitrene ^{3}**2** at 445 nm (50 min, 100 mW, Kr matrix at 15 K). B3LYP/6-311+G(2d,p) computed IR spectrum of: (b) triplet nitrene ^{3}**2**; and (d) benzazirine **3s**.

Relevant for the present investigation was the identification of the first OH stretching overtone in the near-IR spectra. Upon irradiation of matrix-isolated **1** at 255 nm, the IR bands due to the 2ν(OH) and ν(OH) modes of ^{3}**2** were identified at 7051 and 3612 cm^{-1}, in a reasonable match with the corresponding anharmonic B3LYP/SNSD computed absorptions at 7099 and 3634 cm^{-1} (Fig. 2; see also Fig. S3). After consumption of almost all ^{3}**2** by irradiation at 445 nm, the IR bands due to the 2ν(OH) and ν(OH) modes of **3s** were identified at 7054 and 3612 cm^{-1}, having the corresponding anharmonic B3LYP/SNSD computed absorptions at 7103 and 3636 cm^{-1} (Fig. 2). Although the ν(OH) absorption of **3s** and ^{3}**2** is practically coincident, the 2ν(OH) absorption of **3s** is shifted by +3 cm^{-1} in relation to ^{3}**2**, thus being fairly well reproduced by the anharmonic computations, which estimate a shift of +4 cm^{-1}.

The IR-induced chemistry of benzazirine **3s** was then explored by selective vibrational excitation of its OH antenna. A sample of **3s** (Kr, 15 K) was irradiated with narrowband (FWHM ≈ 0.2 cm^{-1}) IR-light, provided by an optical parametric oscillator pumped with a pulsed Nd:YAG laser, tuned at its 2ν(OH) frequency of 7054 cm^{-1}. Monitoring the process after 30 min, by IR spectroscopy, reveals a large-scale conversion (> 50 %) of **3s** into the cyclic ketenimine *anti*-3,7-difluoro-5-hydroxy-1-aza-1,2,4,6-cycloheptatetraene **4a**.[35] The negative and positive bands in the experimental difference IR spectrum are in excellent agreement with the B3LYP/6-311+G(2d,p) computed IR spectra of **3s** and **4a**, respectively (Fig. 3). The

depleted IR bands correspond to those previously identified for **3s** (assigned in Table S2); e.g. matching the most representative ones observed at 1620, 1316, 1201, 1144, 1118/1111, 934/932 cm^{-1}. The most intense emerging IR bands were observed at 1592/1584, 1542/1536, 1426, 1306, 1217 and 1139 cm^{-1}, which are in good correspondence with the most intense computed IR bands of **4a** at 1581 [ν(C=C)], 1525 [ν(C=C)], 1419 [δ(OH), ν(C-C), δ(CH)], 1293 [$\nu(C{=}C{=}N)_s$], 1196 [ν(CF)] and 1133 [ν(CO)] cm^{-1}. The characteristic absorption due to the $\nu(C{=}C{=}N)_s$ mode of **4a** is identified at 1823 cm^{-1}, near the absorption frequency previously reported for the 3,7-difluoro-1-aza-1,2,4,6-cycloheptatetraene analog (1830 cm^{-1}, Ar matrix at 10 K).[32] The 2ν(OH) and ν(OH) bands of **4a** were observed at 7038 and 3605 cm^{-1} (Fig. S4). The presence of the *syn*-OH conformer **4s** can be safely excluded, as some of its distinctive computed IR bands have no correspondence in the experimental IR spectrum (Fig. S5). A detailed assignment of the experimental IR spectrum of **4a** is provided in Table S3.

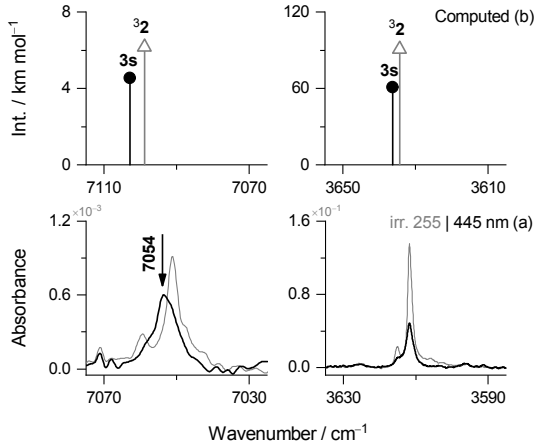

Fig. 2. (a) Selected regions of the experimental near-IR (left) and mid-IR (right) spectra: (gray line) after irradiation of azide **1** at 255 nm (8 min, 30 mW, Kr matrix at 15 K) and production of triplet nitrene ^{3}**2**; (black line) after irradiation of ^{3}**2** at 445 nm (50 min, 100 mW, Kr matrix at 15 K) and production of benzazirine **3s**. (b) Anharmonic wavenumbers and IR intensities computed at the B3LYP/SNSD level for the 2ν(OH) (left) and ν(OH) (right) modes of ^{3}**2** (triangles) and **3s** (circles).

To better understand the experimental observations, we computed the potential energy surface around benzazirine **3s** (Fig. 4). At the CCSD(T)/cc-pVTZ//B3LYP/6-311+G(2d,p) level, the OH-rotamerization barrier of **3a** to the most stable conformer **3s** is 1.8 kcal mol^{-1}, whereas the barrier of **4s** to the most stable **4a** is 3.5 kcal mol^{-1}. With such low-energy barriers, fast OH-rotamerization tunneling is expected to preclude the isolation of the higher-energy conformers **3a** and **4s**, as it has been reported for other phenol derivatives studied in noble-gas matrices.[36–39] Indeed, tunneling calculations using the Wentzel–Kramers–Brillouin model (see details in SI) estimate very short half-lives for **3a** [$\tau_{1/2}$ ~10^{-7} s] and **4s** [$\tau_{1/2}$ ~10^{-4} s], which justify the exclusive identification of benzazirine **3s** and ketenimine **4a** in the performed experiments. In this regard, it is likely that the IR vibrational excitation of **3s** induces ring-expansion to **4s**, which then undergoes fast OH-rotamerization tunneling to the observed product **4a**. At the CCSD(T)/cc-pVTZ//B3LYP/6-311+G(2d,p) level, the ring-expansion barrier of **3s** to **4s** is 10.1 kcal mol^{-1} (well below the ~20 kcal mol^{-1} of vibrational energy deposited in **3s**).

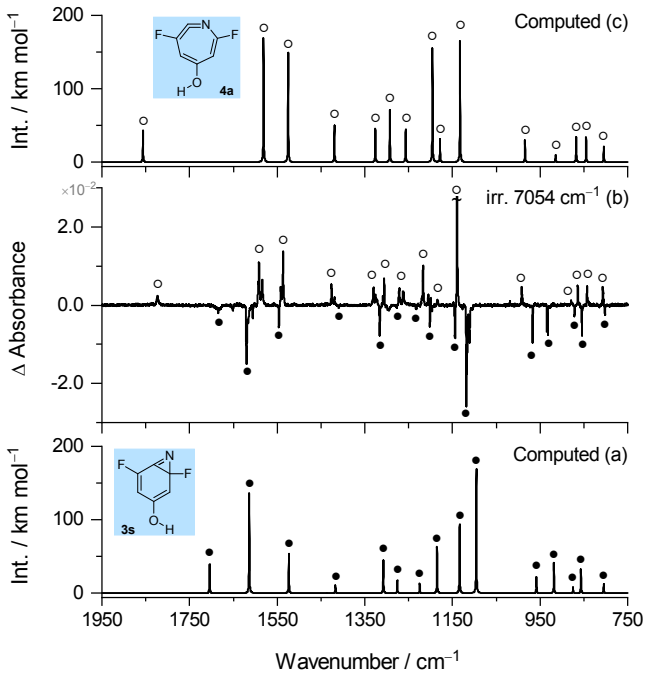

Fig. 3. B3LYP/6-311+G(2d,p) computed IR spectrum of: (a) benzazirine **3s**; and (c) cyclic ketenimine **4a**. (b) Experimental difference IR spectrum showing changes after irradiation at 7054 cm^{-1} (30 min, 100 mW, Kr matrix at 15 K), subsequent to the production of **3s** by irradiation of ^{3}**2** at 455 nm. The downward bands are due to consumed species assigned to **3s** (closed circles). The upward bands are due to the produced species assigned to **4a** (open circles).

Another possible bond-breaking/bond-forming reaction that could result from the vibrational excitation of **3s** is the ring-opening to open-shell singlet nitrene ^{1}A''-**2**, which subsequently should be followed by fast intersystem crossing to triplet ground state ^{3}**2**. Since ^{1}A''-**2** cannot be correctly described with a single-determinant wavefunction, computations were also carried out with multiconfigurational methods (see details in SI). At our best available MRMP/cc-pVTZ//CASSCF(8,8)/cc-pVTZ level, the ring-opening barrier of **3s** to ^{1}A''-**2** is 7.2 kcal mol^{-1}, whereas the ring-expansion barrier of **3s** to **4s** is 4.8 kcal mol^{-1} (such barriers are most probably underestimated by 3–5 kcal mol^{-1}, judging by the MRMP/cc-pVTZ//CASSCF(8,8)/cc-pVTZ underestimation of ~4 kcal mol^{-1} found for the reaction of the 2-fluoro-2*H*-benzazirine **3'** analog to ^{1}A''-**2'** and to **4'**; see Fig. S8).[40] Thus, computations indicate that the IR vibrational excitation of **3s** triggers exclusively the most favorable bond-breaking/bond-forming reaction, i.e. the ring-expansion to **4s**. On the other hand, it is clear that the competitive OH-rotamerization of **3s** to **3a** is a less energetic pathway. However, as mentioned above, **3a** should convert back to **3s** by fast tunneling, making its observation impossible. In any case, remarkably, the existence of this pathway does not preclude the energy deposited into the OH antenna of **3s** to be efficiently transferred to the remote ring-expansion reaction coordinate leading to **4s**.

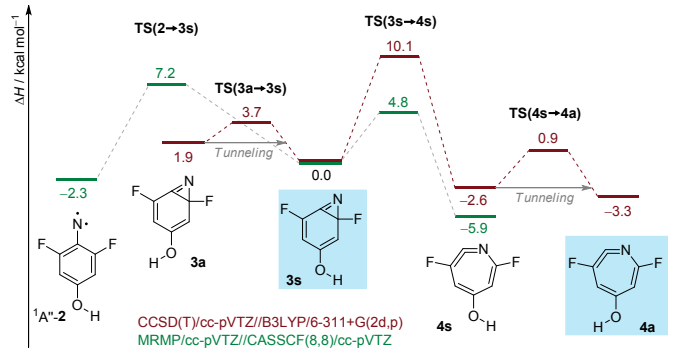

Fig. 4. Reaction pathways for benzazirine **3s** computed at CCSD(T)/cc-pVTZ//B3LYP/6-311+G(2d,p) + ZPVE (red) and MRMP/cc-pVTZ//CASSCF(8,8)/cc-pVTZ + ZPVE (green) levels of theory. ^{1}A'' = open-shell singlet state.

In summary, we demonstrated here that the selective IR vibrational excitation of a remote antenna allows inducing a bond-breaking/bond-forming reaction in an organic molecule, in an efficient way. This accomplishment paves the way for developing a general approach to guide a variety of molecular structure manipulations using IR-light. Harnessing the power of vibrationally induced chemistry creates unprecedented opportunities for highly-selective transformations, in ways not attainable by thermal or electronic excitation processes.

This work was supported by Project POCI-01-0145-FEDER-028973, funded by FEDER, via Portugal 2020 - POCI, and by National Funds via the Portuguese Foundation for Science and Technology (FCT). The CQC is funded by the FCT through the projects UIDB/QUI/00313/2020 and UIDP/QUI/00313/2020. C.M.N. thanks the FCT for an Auxiliary Researcher grant. N.A.M.P. acknowledges the Project POCI-01-0145-FEDER-028973 for a Junior Researcher grant. L.P.V. acknowledges CQC for a Junior Researcher grant. José P. L. Roque is acknowledged for the participation in preliminary experiments.

Conflicts of interest

There are no conflicts to declare

Notes and references

1 K. Heyne and O. Kühn, *J. Am. Chem. Soc.*, 2019, **141**, 11730–11738.
2 F. F. Crim, *Acc. Chem. Res.*, 1999, **32**, 877–884.
3 R. N. Zare, *Science*, 1998, **279**, 1875–1879.
4 V. S. Letokhov, *Nature*, 1983, **305**, 103–108.
5 C. M. Nunes, I. Reva and R. Fausto, *Phys. Chem. Chem. Phys.*, 2019, **21**, 24993–25001.
6 L. Khriachtchev, J. Lundell, E. Isoniemi and M. Räsänen, *J. Chem. Phys.*, 2000, **113**, 4265–4273.
7 R. Fausto, L. Khriachtchev and P. Hamm, in *Physics and Chemistry at Low Temperatures*, ed. L. Khriachtchev, Pan Stanford Publishing, United States, 2011, pp. 51–84.
8 R. Schanz, V. Boţan and P. Hamm, *J. Chem. Phys.*, 2005, **122**, 044509.
9 I. Reva, C. M. Nunes, M. Biczysko and R. Fausto, *J. Phys. Chem. A*, 2015, **119**, 2614–2627.
10 M. Pettersson, J. Lundell, L. Khriachtchev and M. Räsänen, *J. Am. Chem. Soc.*, 1997, **119**, 11715–11716.
11 S. V. Ryazantsev, V. I. Feldman and L. Khriachtchev, *J. Am. Chem. Soc.*, 2017, **139**, 9551–9557.
12 A. Sharma, I. Reva and R. Fausto, *J. Am. Chem. Soc.*, 2009, **131**, 8752–8753.
13 C. M. Nunes, L. Lapinski, R. Fausto and I. Reva, *J. Chem. Phys.*, 2013, **138**, 125101.
14 G. Bazsó, G. Magyarfalvi and G. Tarczay, *J. Phys. Chem. A*, 2012, **116**, 10539–10547.
15 I. Reva, M. J. Nowak, L. Lapinski and R. Fausto, *J. Chem. Phys.*, 2012, **136**, 064511.
16 A. J. Lopes Jesus, I. Reva, C. Araujo-Andrade and R. Fausto, *J. Am. Chem. Soc.*, 2015, **137**, 14240–14243.
17 We have further extended that strategy and introduced the concept of interchangeable remote vibrational antennas. See: A. J. Lopes Jesus, C. M. Nunes, R. Fausto and I. Reva, *Chem. Commun.*, 2018, **54**, 4778–4781.
18 C. M. Nunes, N. A. M. Pereira, I. Reva, P. S. M. Amado, M. L. S. Cristiano and R. Fausto, *J. Phys. Chem. Lett.*, 2020, **11**, 8034–8039.
19 To the best of our knowledge only one other type of organic reaction, involving small ethylene derivatives aggregated with F_2, have been reported in a similar context, see: (a) H. Frei and G. C. Pimentel, *Ann. Rev. Phys. Chem.*, 1985, **36**, 491–524 and references cited therein. For an example of a H-tunnelling reaction switched by conformation control upon IR vibrational excitation see: (b) J. P. L. Roque, C. M. Nunes, L. P. Viegas, N. A. M. Pereira, T. M. V. D. Pinho e Melo, P. R. Schreiner and R. Fausto, *J. Am. Chem. Soc.*, 2021, **143**, 8266–8271.
20 Note that several examples have been reported regarding the vibrational control of bimolecular reactions (mode and bond selectivity) with CH_4 (and isotopically substituted analogs) + atoms (H, O, F, Cl, etc.) and with H_2O (and isotopically substituted analogs) + atoms (H, O, F, Cl, etc.). See for instance: K. Liu, *Annu. Rev. Phys. Chem.,* 2016, **67**, 91–111 and references cited therein.
21 F. Liu, J. M. Beames, A. S. Petit, A. B. McCoy and M. I. Lester, *Science.*, 2014, **345**, 1596–1598.
22 J. Matthews, J. L. Fry, C. M. Roehl, P. O. Wennberg and A. Sinha, *J. Chem. Phys.*, 2008, **128**, 1–13.
23 S. Leytner, D. L. Snavely and O. Grinevich, *Chem. Phys. Lett.*, 1997, **277**, 443–449.
24 D. L. Snavely, O. Grinevich, S. Hassoon and G. Snavely, *J. Chem. Phys.*, 1996, **104**, 5845–5851.
25 T. Stensitzki, Y. Yang, V. Kozich, A. A. Ahmed, F. Kössl, O. Kühn and K. Heyne, *Nat. Chem.*, 2018, **10**, 126–131.
26 J. Y. Shin, M. A. Shaloski, F. F. Crim and A. S. Case, *J. Phys. Chem. B*, 2017, **121**, 2486–2494.
27 M. C. Larsen and V. Vaida, *J. Phys. Chem. A*, 2012, **116**, 5840–5846.
28 T. Schleif, J. Mieres-Perez, S. Henkel, E. Mendez-Vega, H. Inui, R. J. McMahon and W. Sander, *J. Org. Chem.*, 2019, **84**, 16013–16018.
29 C. M. Nunes, A. K. Eckhardt, I. Reva, R. Fausto and P. R. Schreiner, *J. Am. Chem. Soc.*, 2019, **141**, 14340–14348.
30 N. P. Gritsan and M. S. Platz, *Chem. Rev.*, 2006, **106**, 3844–3867.
31 N. P. Gritsan, A. D. Gudmundsdóttir, D. Tigelaar, Z. Zhu, W. L. Karney, C. M. Hadad and M. S. Platz, *J. Am. Chem. Soc.*, 2001, **123**, 1951–1962.
32 J. Morawietz and W. Sander, *J. Org. Chem.*, 1996, **61**, 4351–4354.
33 For the UV-Vis spectrum of the 2,6-difluorophenylnitrene ^{3}**2'** see: C. Carra, R. Nussbaum and T. Bally, *ChemPhysChem*, 2006, **7**, 1268–1275.
34 An unidentified product in a minor amount was found to have IR absorptions at 1664, 1350, 1189, 996 and 884 cm^{-1}.
35 As expected, IR-light irradiations tuned at a frequency outside the range of the OH stretching overtone of **3s** (e.g. at 7036 cm^{-1} where no vibrational transitions are expected) did not lead to any transformation.
36 A. J. Lopes Jesus, I. Reva, C. M. Nunes, J. P. L. Roque, S. M. V. Pinto and R. Fausto, *Chem. Phys. Lett.*, 2020, **747**, 137069.
37 A. J. Lopes Jesus, C. M. Nunes, I. Reva, S. M. V. Pinto and R. Fausto, *J. Phys. Chem. A*, 2019, **123**, 4396–4405.
38 S. Nanbu, M. Sekine and M. Nakata, *J. Mol. Struct.*, 2012, **1025**, 69–73.
39 S. Nanbu, M. Sekine and M. Nakata, *J. Phys. Chem. A*, 2011, **115**, 9911–9918.
40 We have previously found that NEVPT2 computations also underestimated in 4–5 kcal mol^{-1} the ring-expansion barrier of a benzazirine to a cyclic ketenimine, whereas CCSD(T) computations provided a good rationalization for the experimental observations (see ref. 29). Here, we also found that CCSD(T) computations for the ring-expansion barrier of **3'** to **4'** is in excellent agreement with the experimental results (see Fig. S8).

Table of contents information

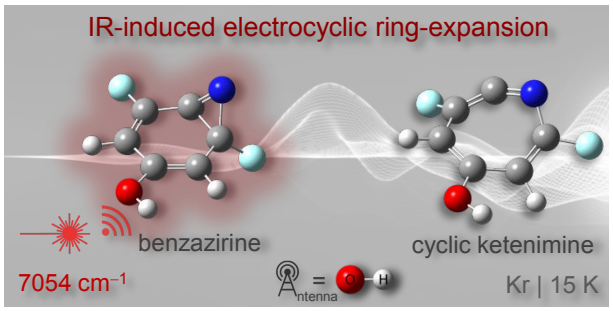

Electrocyclic ring-expansion of a benzazirine induced by near-IR light tuned at the overtone stretching frequency of its OH remote antenna. A proof-of-principle demonstration to harnessing the power of IR vibrational excitation to guide molecular reactions in unprecedent selective way.

Inducing Molecular Reactions by Selective Vibrational Excitation of a Remote Antenna with Near-Infrared Light

Cláudio M. Nunes,* Nelson, A. M. Pereira, Luís P. Viegas, Teresa M. V. D. Pinho e Melo, and Rui Fausto

University of Coimbra, CQC, Department of Chemistry, 3004-535 Coimbra, Portugal

Email: cmnunes@qui.uc.pt

Supporting Information (SI)

Table of Contents:

1. Experimental and Computational Methods

Synthesis of 2,6-Difluoro-4-Hydroxyphenylazide:

Commercial reagents were used as purchased. ^{1}H, ^{13}C and ^{19}F Nuclear Magnetic Resonance (NMR) spectra were recorded on an NMR spectrometer Bruker Avance III operating at 400, 100 and 376.5 MHz, respectively. Chemical shifts are referred to the residual signal of DMSO-d_6 or to the internal standard tetramethylsilane (TMS). Chemical shifts are given in parts per million (ppm) relative to TMS and coupling constants *J* are given in Hertz. Thin-layer chromatography (TLC) was carried out on silica gel 60 F_{254} plates (AL TLC 20x20). Column chromatography was performed on Silica Gel 60 (0.04 - 0.063 mm).

The azide **1** was prepared according to an adapted procedure described for other similar derivatives.[S1]

4-Amino-3,5-difluorophenol (300 mg, 2.1 mmol) was dissolved in trifluoroacetic acid (3 ml) and the solution was cooled in an ice bath. Sodium nitrite (171 mg, 2.5 mmol) was added portionwise with stirring over 5 minutes followed by the addition of sodium azide (171 mg, 2.6 mmol). The solution was allowed to stir for an additional 1 h. Then, water (25 ml) was added, and the reaction mixture was extracted with ethyl acetate (3 x 25 ml), washed well with water and saturated aqueous $NaHCO_3$. The extract was dried over anhydrous sodium sulfate and the solvent evaporated *in vacuo* to yield a dark oil. This residue was purified by column chromatography (silica gel; eluent: hexane /ethyl acetate, 3:1) to give, after removing the solvent, the desired azide **1** as a brown oil (180 mg, 51% yield). Exposure to light or kept the product at room temperature results in degradation and, therefore, it should be stored in the dark below room temperature (< −10 ºC) to minimize its decomposition.

^{1}H NMR (400 MHz, DMSO_d_6): δ (ppm) 10.42 (bs, 1H, OH), 6.60-6.53 (m, 2H, Ph-H). ^{13}C NMR (100 MHz, DMSO_d_6): δ (ppm) 155.6 (t, J = 14.0 Hz), 155.5 (dd, J = 245.6, 7.8 Hz), 106.9 (t, J = 15.1 Hz), 100.2-99.9 (m). ^{19}F NMR (376.5 MHz, DMSO_d_6): δ (ppm) −123.12 (s, 2F). IR (Kr matrix, 15 K) wavenumber (cm^{-1}): 621 (w), 651 (w), 704 (vw), 790 (w), 817 (w), 843 (w), 1002 (w), 1049 (s), 1118 (m), 1138 (w), 1144/1145 (w), 1231/1232 (m), 1300/1303 (m), 1321/1327 (br), 1380 (vw), 1462 (w), 1480 (w), 1513 (s), 1516 (w), 1606 (w, H_2O), 1628 (w), 1648 (w), 2083 (w), 2104 (w), 2135 (s), 3626 (m) and 7080 (vw).

Matrix Isolation Spectroscopy: A sample of azide **1** was placed in a glass tube that was then connected to a stainless-steel needle valve (SS4 BMRG valve NUPRO) attached to the vacuum chamber of a cryostat (APD Cryogenics closed-cycle refrigerator with DE-202A expander). For the preparation of the matrices, the sample vapors (at room temperature) were deposited together with a large excess of krypton (N48, Air Liquide) onto a CsI window at 15 K. The temperature was measured directly at the sample holder window by a silicon diode sensor connected to a digital controller (LakeShore 331), providing stabilization accuracy of 0.1 K. Infrared spectra were recorded using a Thermo Nicolet 6700 Fourier transform infrared (FTIR) spectrometer, equipped with a deuterated triglycine sulfate (DGTS) detector and a KBr beam splitter, for the mid-IR range (4000–400 cm^{-1}), or with a thermoelectrically cooled indium gallium arsenide (InGaAs) detector and a CaF_2 beam splitter, for the near-IR range (7500−4000 cm^{-1}). The infrared spectra were recorded with resolution 0.5 and 2 cm^{-1} in the mid-IR and near IR ranges, respectively. Modifications of the sample compartment of the spectrometer were done to accommodate the cryostat head and allow purging of the instrument by a stream of dry air to avoid interference from atmospheric H_2O and CO_2.

Irradiation Experiments: The matrix-isolated species were irradiated through a quartz window of the cryostat, using frequency-tunable narrowband light (full width at half-maximum [FWHM] ≈ 0.2 cm^{-1}) provided by a frequency-doubled signal (UV range), a signal (visible range) or an idler (near-IR range) beam of an optical parametric oscillator (Spectra Physics Quanta-Ray MOPO-SL) pumped with a pulsed Nd:YAG laser (Spectra-Physics PRO-230: output power ≈ 4.3 W; wavelength = 355 nm; duration = 10 ns; repetition rate =10 Hz).

IR Spectra Computations: To support the assignment of the experimental mid-IR spectra, geometry optimizations and harmonic frequency computations were performed at the B3LYP/6-311+G(2d,p) level of theory,[S2–S5] using Gaussian 16 (Revision B.01)[S6] software package. All computations were performed using the tight optimization criteria and an ultrafine integration grid. The nature of stationary points was confirmed by the analysis of the Hessian matrices. In order to correct for the neglected anharmonic effects, incomplete treatment of electron correlation, and basis set limitations, the harmonic vibrational frequencies were scaled by a factor of 0.979.[S7] The scaled harmonic vibrational frequencies

and the respective absolute intensities were used to simulate the IR spectra by convoluting each peak with a Lorentzian function (FWHM = 1 cm^{-1}). In this case, the integral band intensities correspond to the calculated infrared absolute intensities in units of km mol^{-1}.

To support the assignment of the experimental OH stretching fundamentals and first overtones, geometry optimizations and anharmonic frequency computations, using the fully automated generalized second-order vibrational perturbative theory (GVPT2),[S8–S9] were performed at the B3LYP/SNSD[10] level of theory, using Gaussian 16 (Revision B.01). All computations were performed using the very tight optimization criteria and a superfine integration grid.

Computations of the PES: The single-point energy coupled-cluster calculations with singles, doubles, and perturbative triples [CCSD(T)] were performed with the cc-pVTZ basis set[S11] and through the algorithms[S12–S14] present in the GAMESS-US package[S15]. Such calculations were based on geometries optimized at the B3LYP/6-311+G(2d,p) level of theory. Multireference calculations were performed with the CASSCF method[S16–S19] employing an active space consisting of eight electrons and eight orbitals and executed with the cc-pVTZ basis set, hereafter designated CASSCF(8,8)/cc-pVTZ level of theory, using the GAMESS-US package. Following the approach used in the CASSCF calculations of fluorinated derivatives of phenylnitrene,[S20] the eight orbitals included in the active space were selected to be analogous to those used in similar calculations involving the ring expansion of phenylnitrene[S21]. For example, for **2** the (8,8) active space consisted of seven π and π^* molecular orbitals (MOs), plus the in-plane p atomic orbital on nitrogen. For **4** species, the four π and the four π^* MOs of the double bonds were used. For all transition states and also for **3**, the active space consisted of six MOs mainly π in character plus a $\sigma/\sigma*$ pair. Dynamical correlation was added to the CASSCF results via multireference Møller-Plesset MRMP(8,8)/cc-pVTZ calculations[S22–S25] using the geometries previously optimized at the CASSCF(8,8)/cc-pVTZ level of theory.

Tunneling Rates Computations: Tunneling computations were performed based on B3LYP/6-311+G(2d,p) computed potential energy profiles along the intrinsic reaction coordinate (IRC) in non-mass-weighted Cartesian coordinates (expressed in units of Bohr).[S26] The transmission coefficients for H-atom tunneling through a parabolic barrier

were computed using the Wentzel−Kramers−Brillouin (WKB) approximation.[S27–S29] Accordingly, the probability *P(E)* of tunneling is given by equation (1):[S30]

$$P(E) = e^{-\pi^2 w\sqrt{2m(V_0-E)}/h} \qquad (1)$$

where a particle with mass *m* tunnels through a barrier with height V_0 and width *w*, (V_0−*E*) is the energy deficiency of the particle with respect to the top of the barrier, and *h* is the Planck's constant. For the OH-rotamerization **3a→3s**, the computed probability of tunneling was estimated equal to 4.8×10^{-6}, using the calculated barrier height of 7.8 kJ mol^{-1} (1.9 kcal mol^{-1}) and width at the ZPVE level of 2.37 Bohr (Figure S6). The tunneling rate is the product of the probability of tunneling (transmission coefficient) and the frequency of attempts. If the H-atom of the OH moiety of **3a** is vibrating at a τ(OH) torsional frequency of about 214 cm^{-1} [B3LYP/6-311+G(2d,p) computed value] this results in a tunneling rate of 3.1×10^{7} s^{-1}, *i.e.* a half-life time of 2.3×10^{-8} s. For the OH-rotamerization **4s→4a**, the computed probability of tunneling was estimated equal to 5.1×10^{-10}, using the calculated barrier height of 16.0 kJ mol^{-1} (3.8 kcal mol^{-1}) and width at the ZPVE level of 2.89 Bohr (Figure S7). If the H-atom of the OH moiety of **4s** is vibrating at a τ(OH) torsional frequency of about 348 cm^{-1} [B3LYP/6-311+G(2d,p) computed value], this results in a tunneling rate of 5.3×10^{3} s^{-1}, *i.e.* a half-life time of 1.3×10^{-4} s.

2. Figures

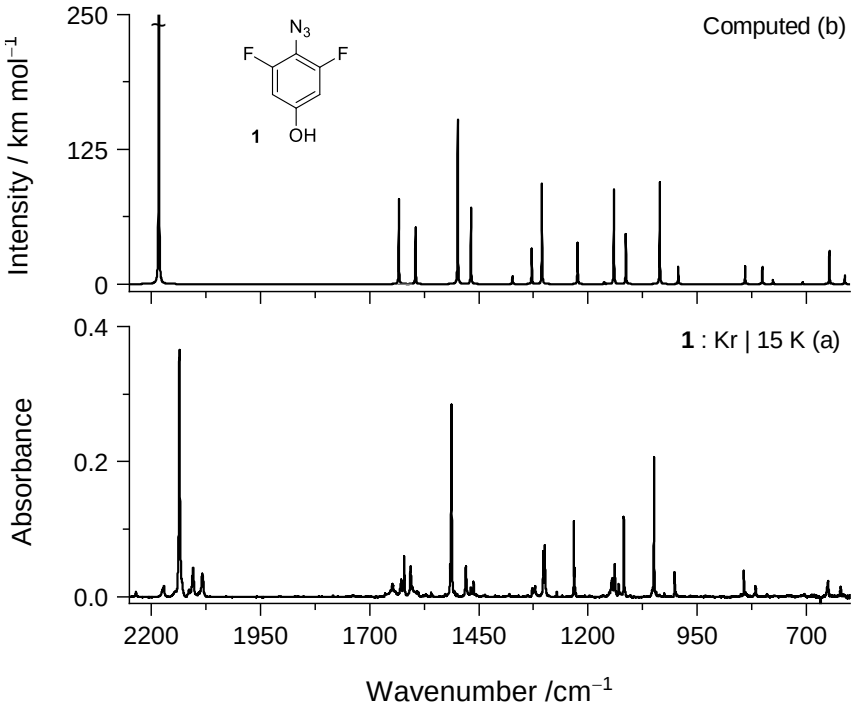

Figure S1. (a) Experimental IR spectrum of azide **1** isolated in a Kr matrix at 15 K. (b) B3LYP/6-311+G(2d,p) computed IR spectrum azide **1**. Selected regions of the near-IR and mid-IR spectra showing the 2ν(OH) and ν(OH) modes of **1** are provided in Figure S3.

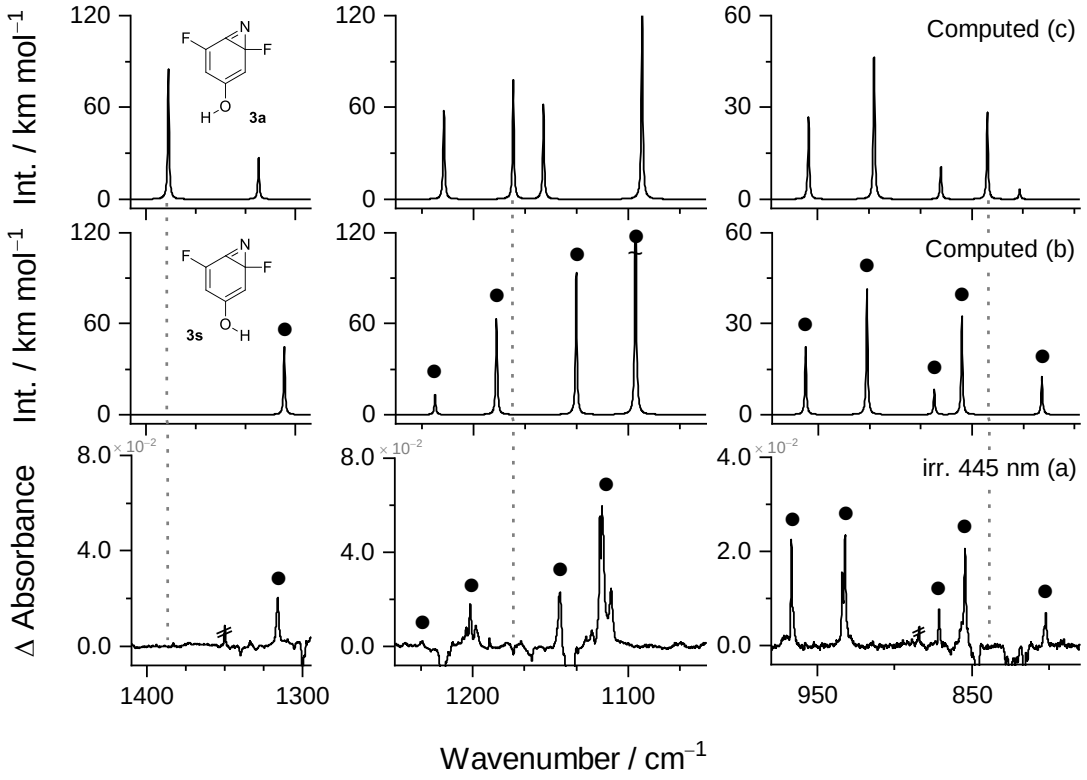

Figure S2. (a) Experimental difference IR spectrum showing changes after irradiation of triplet nitrene ^{3}**2** at 445 nm (50 min, 100 mW, Kr matrix at 15 K). The upward bands signed with closed circles (●) are due to the produced benzazirine **3s**. The upward bands signed with double line are due to a minor amount of an unidentified product. (b,c) B3LYP/6-311+G(2d,p) computed IR spectra of *syn*-OH **3s** and *anti*-OH **3a**. Vertical dotted lines indicate the absence of distinctive computed IR bands of **3a** in the experimental IR spectrum.

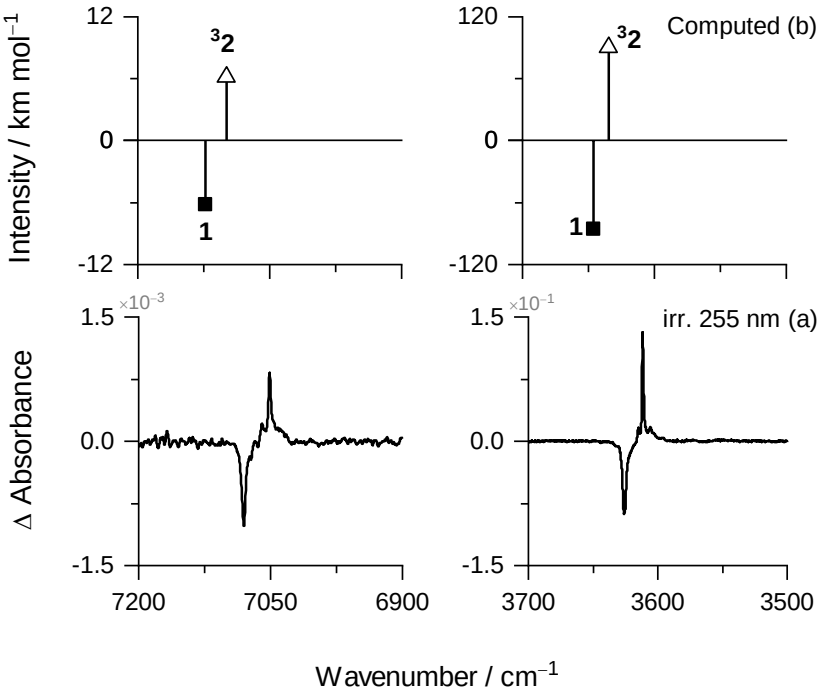

Figure S3. (a) Selected regions of the experimental difference near-IR (left) and mid-IR (right) spectra showing changes resulting from irradiation of azide **1** at 255 nm (8 min, 30 mW, Kr matrix at 15 K). (b) Anharmonic wavenumbers and IR intensities computed at the B3LYP/SNSD level for the 2ν(OH) (left) and ν(OH) (right) modes of azide **1** (squares, intensities multiplied by −1) and of triplet nitrene ^{3}**2** (triangles).

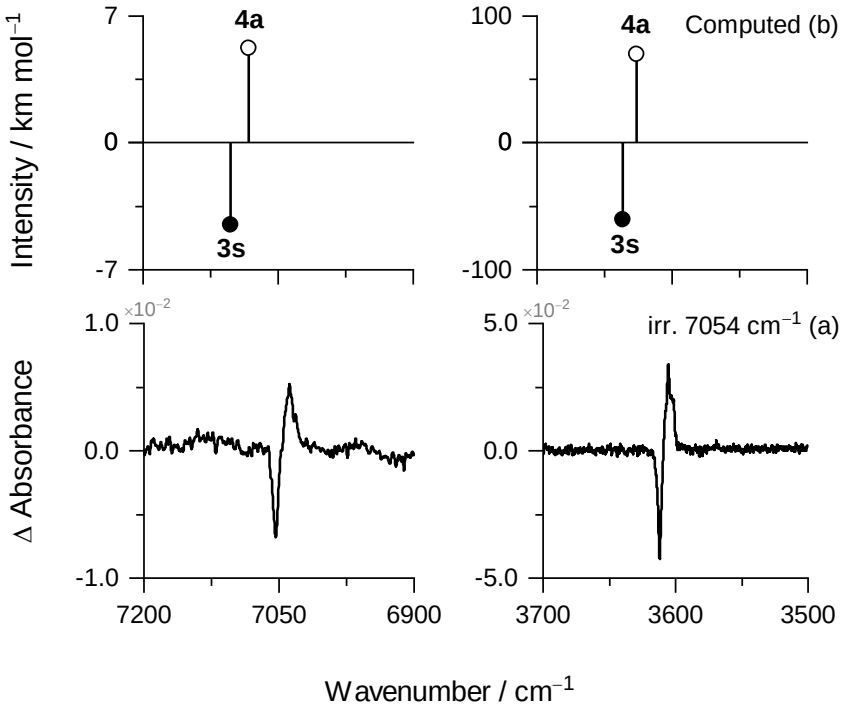

Figure S4. (a) Selected regions of the experimental difference near-IR (left) and mid-IR (right) spectra showing changes resulting from irradiation of benzazirine **3s** at 7054 cm^{-1} (30 min, 100 mW, Kr matrix at 15 K). (b) Anharmonic wavenumbers and IR intensities computed at the B3LYP/SNSD level for the 2ν(OH) (left) and ν(OH) (right) modes of benzazirine **3s** (closed circles, intensities multiplied by −1) and of cyclic ketenimine **4a** (open circles).

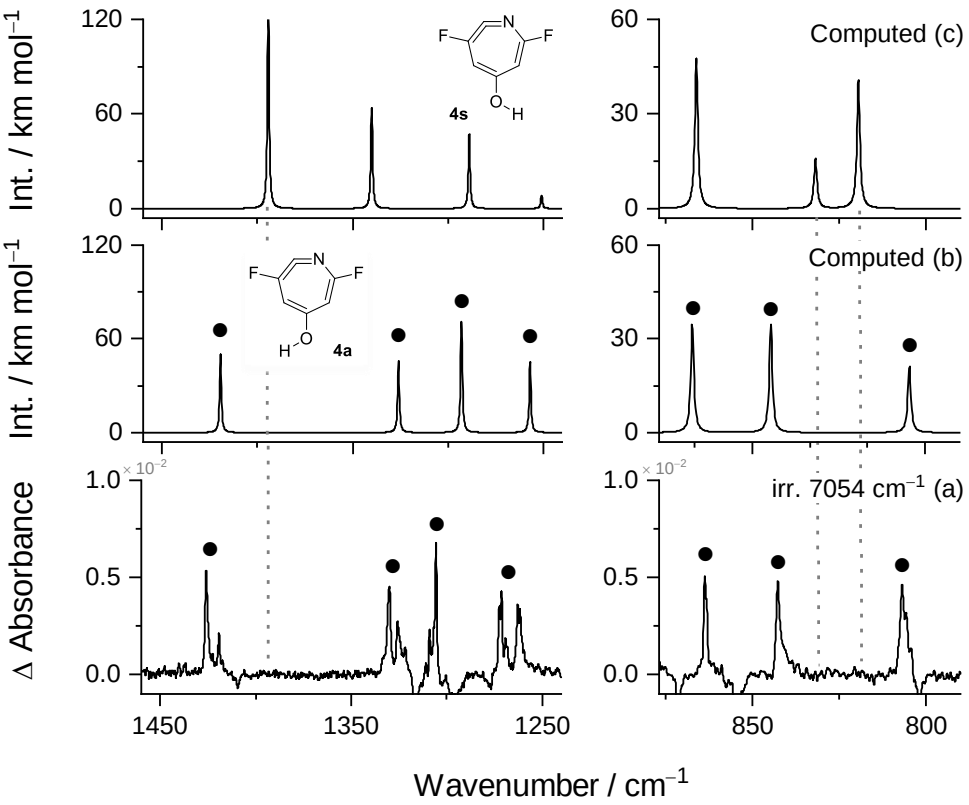

Figure S5. (a) Experimental difference IR spectrum showing changes after irradiation of benzazirine **3s** at 7054 cm^{-1} (30 min, 100 mW, Kr matrix at 15 K). The upward bands signed with closed circles (●) are due to the produced cyclic ketenimine **4a**. (b,c) B3LYP/6-311+G(2d,p) computed IR spectra of *anti*-OH **4a** and *syn*-OH **4s**. Vertical dotted lines indicate the absence of distinctive computed IR bands of **4s** in the experimental IR spectrum.

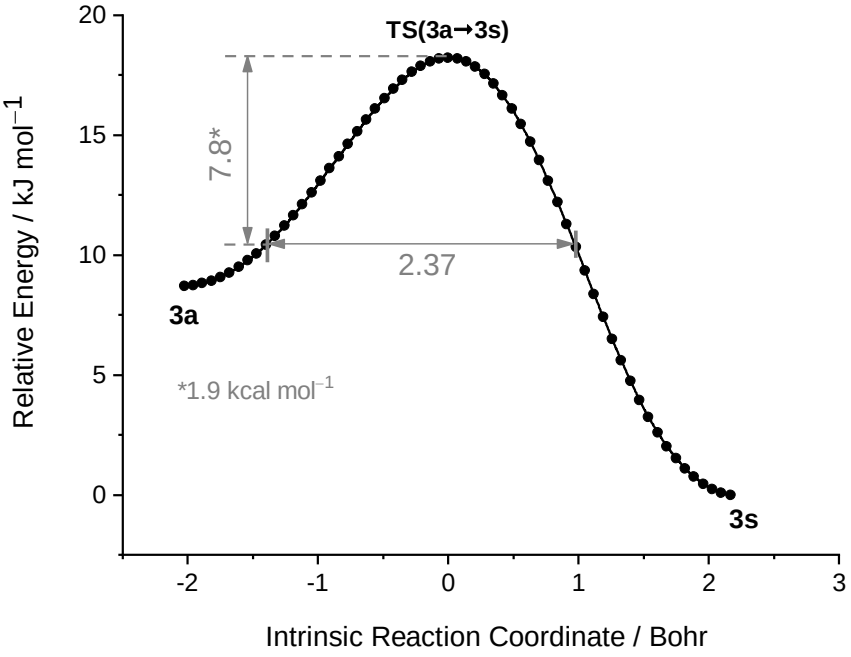

Figure S6. Relative electronic energy as a function of intrinsic reaction coordinate (IRC) for OH-rotamerization of **3a** to **3s** computed at the B3LYP/6-311+G(2d,p) level in non-mass-weighted (Cartesian) coordinates. The vertical arrow designates the B3LYP/6-311+G(2d,p) ZPVE-corrected energy of the reactant **3a** relative to the transition state **TS(3a→3s)** [a similar value was computed at CCSD(T)/cc-pVTZ//B3LYP/6-311+G(2d,p) level, see Figure 4]. The horizontal arrow designates the barrier width considering the ZPVE-corrected energy values of the stationary points superimposed with the pure electronic IRC energy profile.

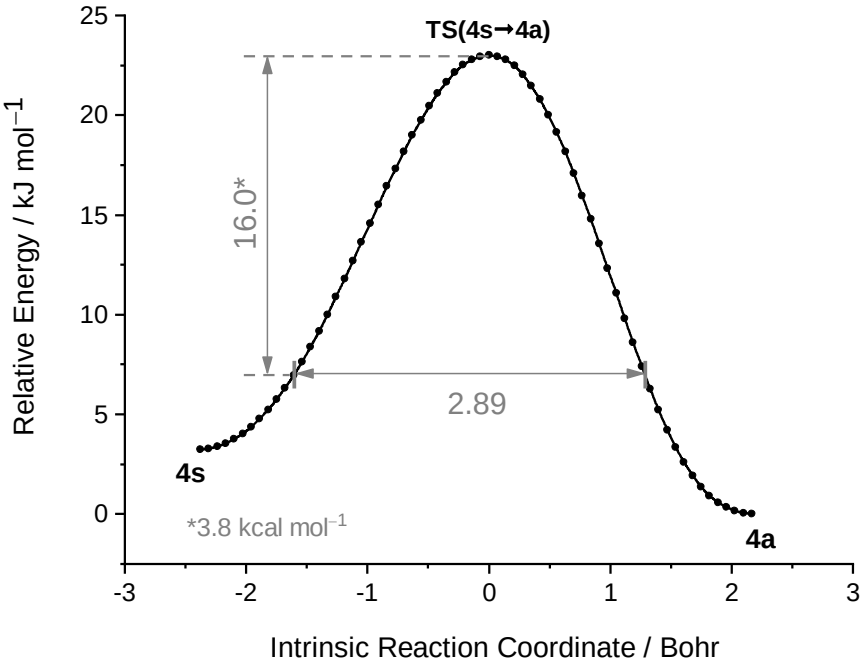

Figure S7. Relative electronic energy as a function of intrinsic reaction coordinate (IRC) for OH-rotamerization of **4s** to **4a** computed at the B3LYP/6-311+G(2d,p) level in non-mass-weighted (Cartesian) coordinates. The vertical arrow designates the B3LYP/6-311+G(2d,p) ZPVE-corrected energy of the reactant **4s** relative to the transition state **TS(4s→4a)** [a similar value was computed at CCSD(T)/cc-pVTZ//B3LYP/6-311+G(2d,p) level, see Figure 4]. The horizontal arrow designates the barrier width considering the ZPVE-corrected energy values of the stationary points superimposed with the pure electronic IRC energy profile.

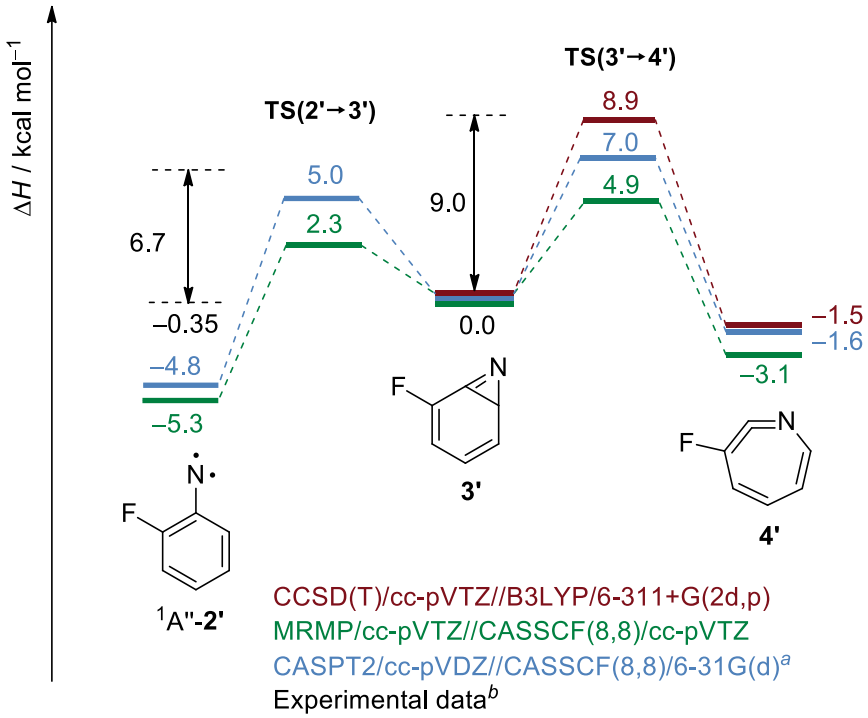

Figure S8. Reaction pathways for 2-fluoro-2*H*-benzazirine **3'** computed at CCSD(T)/cc-pVTZ//B3LYP/6-311+G(2d,p) + ZPVE (red) and MRMP/cc-pVTZ//CASSCF(8,8)/cc-pVTZ + ZPVE (green) levels of theory. ^{1}A" = open-shell singlet state. ^{a}Computed data at CASPT2/cc-pVDZ//CASSCF(8,8)/6-31G(d) + ZPVE (blue) level of theory were taken from ref. S20. ^{b}The experimental data refers to results obtained from laser flash photolysis experiments taken from ref. S20; the activation energies were measured using Arrhenius plots and the energy difference between **2'** and **3'** was obtained from an estimated equilibrium constant. Note that this PES is rather unusual because the **TS(2'→3')** is less energetic than **TS(3'→4')**, and therefore, it allowed the measurement of the activation energy for the ring-expansion of a benzazirine to a cyclic ketenimine (see ref. S20).

3. Nuclear Magnetic Resonance Spectra.

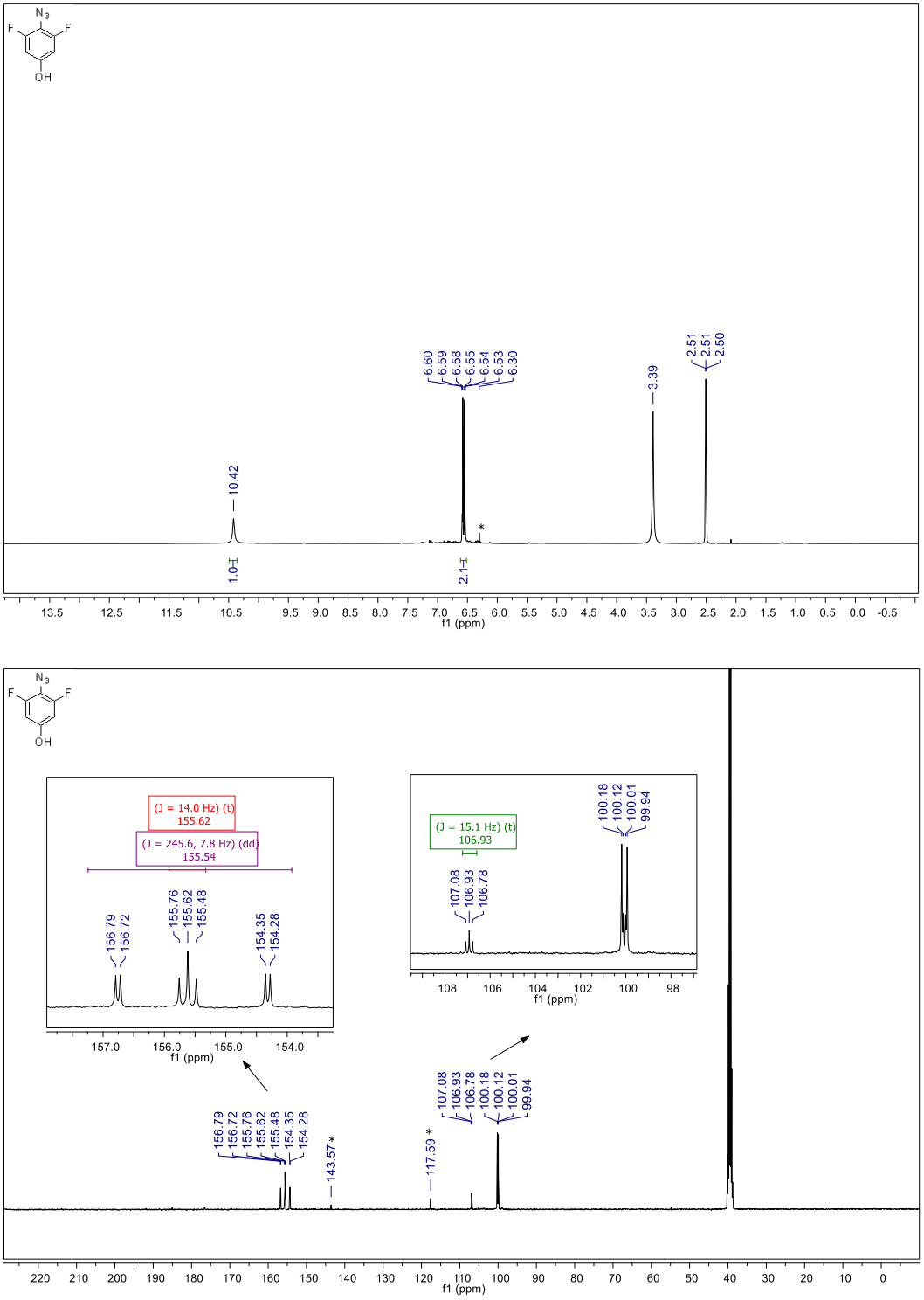

Figure S9a. ^{1}H (upper) and ^{13}C (down) NMR spectra of 2,6-difluoro-4-hydroxyphenylazide (**1**) in DMSO-d_6. *These traces of contaminants should have resulted due to instability of azide **1** under the room temperature conditions of the NMR experiments.

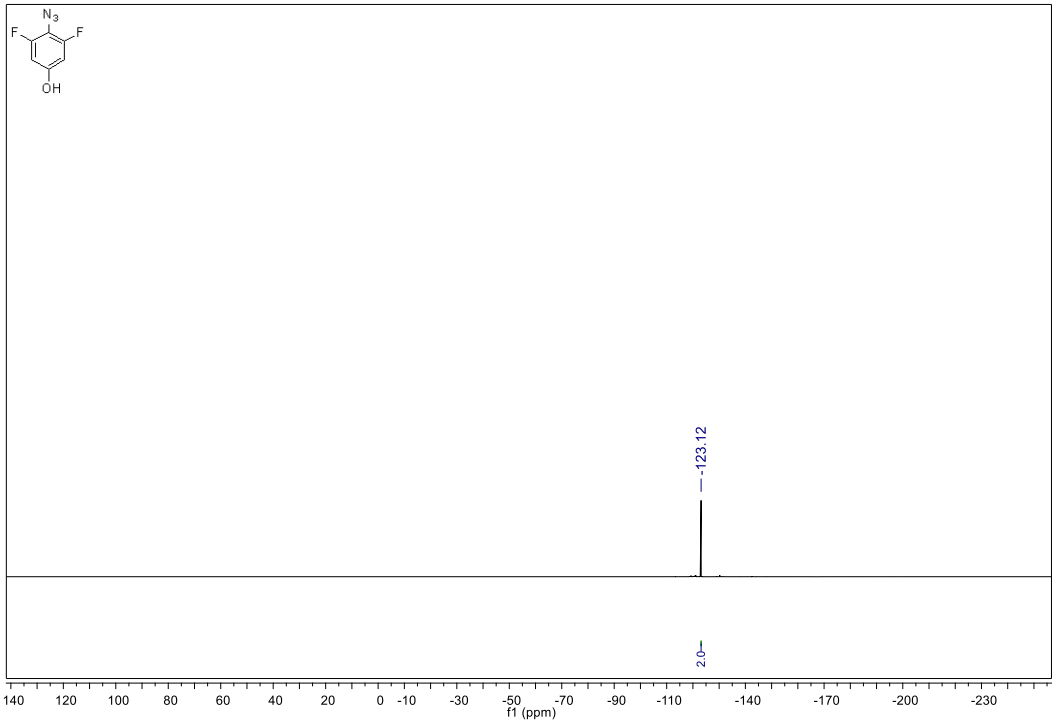

Figure S9b. ^{19}F NMR spectra of 2,6-difluoro-4-hydroxyphenylazide (**1**) in DMSO-d_6.

4. Tables

Table S1. Experimental IR spectral data (krypton matrix at 15 K), B3LYP/6-311+G(2d,p) calculated vibrational frequencies (ν, cm^{-1}), absolute infrared intensities (A^{th}, km mol^{-1}), and vibrational assignment of triplet 2,6-difluoro-4-hydroxyphenylnitrene ^{3}**2**.[a]

Kr matrix[b]		Calculated[c]		Approx. assignment[e]
ν	I	ν	A^{th}	
7051	vw	7099[d]	6.1[d]	[2ν(OH)]
3612	s	3634[d]	90.7[d]	[ν(OH)]
-	-	3143	1.4	[ν(CH)1]
-	-	3115	0.6	[ν(CH)2]
1602/1599	s/m	1598	338.9	[$\nu(CC_{ring})$1]
1536	w	1531	44.7	[$\nu(CC_{ring})$2]
1468	s	1453	150.8	[$\nu(CC_{ring})$3]
1421	w	1409	25.9	[$\nu(CC_{ring})$4]
-	-	1322	0.01	$[\nu(CF)]_s$
1300	w	1291	67.0	[δ(OH)]
1289	w	1273	41.6	[ν(C−N)]
1220/1218	s/w	1206	114.6	[δ(CH)1] + [δ(CH)2]; [δ(OH)]
1162	vw	1159	7.8	[δ(CH)2)]; [δ(OH)]
1139/1137	s/m	1134	236.0	[ν(C−O)]; [δ(CH)1]; [δ(OH)]
1018	s	1007	111.9	$[\nu(CF)]_{as}$
994	w	985	16.6	[$\nu(CC_{ring})$5]
846	w	843	28.3	[γ(CH)1]
825	w	811	25.4	[γ(CH)2]
816	vw	806	13.1	[δ(ring)1]
706	vw	713	4.2	[τ(ring)1]
620	vw	614	11.6	[δ(ring)2]
612	vw	606	8.7	[γ(CH)1] + [γ(CH)2]
-	-	565	0.01	[$\nu(CC_{ring})$6]
-	-	550	1.9	[τ(ring)2]
502	w	500	10.6	[δ(ring)3]

[a]Triplet 2,6-difluoro-4-hydroxyphenylnitrene ^{3}**2** was generated by UV-irradiation (λ = 255 nm) of 2,6-difluoro-4-hydroxyphenylazide **1** in a krypton matrix at 15 K. [b]Experimental intensities are presented in qualitative terms: s = strong, m = medium, w = weak and vw = very weak. [c]B3LYP/6-311+G(2d,p) calculated frequencies scaled by a factor of 0.979. [d] B3LYP/SNSD computed anharmonic vibrational frequencies and absolute IR intensities were given for the 2ν(OH) and ν(OH) modes. [e]Assignments made by inspection of Chemcraft[S31] animation. Abbreviations: ν = stretching, δ = in-plane bending, γ = ou-of-plane bending, τ = torsion, s = symmetric, and as = antisymmetric, ring = 6-member ring. Signs "+" and "–" designate combinations of vibrations occurring in "syn"-phase ("+") and in "anti"-phase ("–").

Table S2. Experimental IR spectral data (krypton matrix at 15 K), B3LYP/6-311+G(2d,p) calculated vibrational frequencies (ν, cm^{-1}), absolute infrared intensities (A^{th}, km mol^{-1}), and vibrational assignment of *syn*-2,6-difluoro-4-hydroxy-2*H*-benzazirine **3s**.[a]

Kr matrix[b]		Calculated[c]		Approx. assignment[e]
ν	I	ν	A^{th}	
7054	vw	7103[d]	4.5[d]	[2ν(OH)]
3612	m	3636[d]	60.8[d]	[ν(OH)]
3075	vw	3130	4.2	[ν(CH)1]
		3100	7.4	[ν(CH)2]
1685	w	1704	63.7	[ν(C=N)]
1620	s	1614	218.3	[ν(C=C_{ring})1]
1546	w	1523	87.1	[ν(C=C_{ring})2]
1410	vw	1417	16.8	[δ(OH)]
1316	s	1308	71.8	[δ(CH)1]; [ν(CC_{ring})3]
1277	vw	1276	28.0	[δ(CH)2]; [ν(C−O)
1232	w	1225	21.4	[ν(CC_{ring})4]; [δ(OH)] – [δ(CH)1]
1201	m	1185	99.5	[ν(CF)1; [δ(OH)] + [δ(CH)2]
1144	m	1134	150.1	[ν(C−O)]; [δ(CH)2] + [δ(CH)1] + [δ(OH)]
1118/1117/1111	m/m/m	1095	265.5	[ν(CF)2]; [δ(CH)2]
967	m	958	35.0	[ν(CC_{ring})5]
934/932	m/m	918	67.9	[ν(CC_{ring})6]
871	vw	875	13.6	[γ(CH)1]
854	m	857	51.0	[γ(CH)1] + [γ(CH)2]
802	w	805	19.6	[γ(CH)2] – [γ(CH)1]
750	vw	748	7.5	[γ(CH)2]
628	vw	629	14.1	[τ(ring)1]
609	vw	608	12.8	[τ(ring)2]
-	-	590	0.1	[δ(ring)1]
533	vw	534	7.2	[δ(ring)2]
501	vw	497	7.9	[δ(ring)3]

[a] *syn*-2,6-Difluoro-4-hydroxy-2*H*-benzazirine **3s** was generated by irradiation (λ = 445 nm) of triplet 2,6-difluoro-4-hydroxyphenylnitrene ^{3}**2** in a krypton matrix at 15 K. [b] Experimental intensities are presented in qualitative terms: s = strong, m = medium, w = weak and vw = very weak. [c] B3LYP/6-311+G(2d,p) calculated frequencies scaled by a factor of 0.979. [d] B3LYP/SNSD computed anharmonic vibrational frequencies and absolute IR intensities were given for the 2ν(OH) and ν(OH) modes. [e] Assignments made by inspection of Chemcraft[S31] animation. Abbreviations: ν = stretching, δ = in-plane bending, γ = ou-of-plane bending, τ = torsion, s = symmetric, and as = antisymmetric, ring = 6-member ring. Signs "+" and "–" designate combinations of vibrations occurring in "syn"-phase ("+") and in "anti"-phase ("–").

Table S3. Experimental IR spectral data (krypton matrix at 15 K), B3LYP/6-311+G(2d,p) calculated vibrational frequencies (ν, cm^{-1}), absolute infrared intensities (A^{th}, km mol^{-1}), and vibrational assignment of *anti*-3,7-difluoro-5-hydroxy-1-aza-1,2,4,6-cycloheptatetraene **4a**.[a]

Kr matrix[b]		Calculated[c]		Approx. assignment[e]
ν	I	ν	A^{th}	
7038	vw	7082[d]	5.2[d]	[2ν(OH)]
3605	m	3626[d]	70.1[d]	[ν(OH)]
-	-	3126	1.7	[ν(CH)1]
-	-	3056	14.6	[ν(CH)2]
1823	br	1856	68.7	$[\nu(C{=}C{=}N)_{as}]$
1592/1584	m/w	1581	273.0	$[\nu(C{=}C_{ring})]_{as}$
1542/1536	w/m	1525	238.3	$[\nu(C{=}C_{ring})]_{s}$
1426/1419	w/vw	1419	79.1	$[\delta(OH)]$; $[\nu(CC_{ring})1]$; [δ(CH)2]
1330/1326	w/vw	1326	72.6	[δ(CH)1]
1309/1306	vw/w	1293	113.1	$[\nu(C{=}C{=}N)]_{s}$
1271/1263	w/w	1257	71.3	$[\nu(CC_{ring})2]$; [δ(OH)]
1217	m	1196	244.6	$[\nu(CF)]_{as}$
1184	vw	1178	51.1	[δ(CH)2]; [δ(OH)]
1139	s	1133	261.3	[ν(C−O)]
992	w	984	47.8	$[\nu(CC_{ring})3]$
879	vw	915	15.3	[ν(CN)]
864	w	867	55.4	[δ(ring)1]
843	w	845	54.4	[γ(CH)1]
807	w	805	34.1	[γ(CH)2]
672	w	680	40.6	[τ(ring)1]
654	vw	660	2.5	[γ(CH)1] + [γ(CH)2]
613	vw	613	12.5	[τ(ring)2]
587	vw	585	4.1	[δ(ring)2]

[a] *anti*-3,7-Difluoro-5-hydroxy-1-aza-1,2,4,6-cycloheptatetraene **4a** was generated in a krypton matrix at 15 K by vibrational excitation of *syn*-2,6-difluoro-4-hydroxy-2*H*-benzazirine **3s** at the 2ν(OH) frequency (7054 cm^{-1}). [b] Experimental intensities are presented in qualitative terms: s = strong, m = medium, w = weak, vw = very weak and br = broad. [c] B3LYP/6-311+G(2d,p) calculated frequencies scaled by a factor of 0.979. [d] B3LYP/SNSD computed anharmonic vibrational frequencies and absolute IR intensities were given for the 2ν(OH) and ν(OH) modes [e] Assignments made by inspection of Chemcraft[S31] animation. Abbreviations: ν = stretching, δ = in-plane bending, γ = ou-of-plane bending, τ = torsion, s = symmetric, and as = antisymmetric, ring = 7-member ring. Signs "+" and "–" designate combinations of vibrations occurring in "syn"-phase ("+") and in "anti"-phase ("–").

Table S4. Single-point energies, in Hartree, of the different structures optimized in this work, calculated with CCSD(T) and MRMP(8,8). Both sets of calculations employ the cc-pV*T*Z basis set and are based on B3LYP/6-311+G(2d,p) and CASSCF(8,8)/cc-pV*T*Z geometries, respectively.

Structure	CCSD(T)	MRMP(8,8)
^{1}A″-**2**	-	-559.0606994439
TS(2 → 3s)	-	-559.0457065027
3a	-559.1448326889	-559.0557473358
TS(3a → 3s)	-559.1412854746	-559.0521492235
3s	-559.1483123697	-559.0592186267
TS(3s → 4s)	-559.1303357690	-559.0494607606
4s	-559.1526596941	-559.0684274228
TS(4s → 4a)	-559.1454870607	-559.0625230406
4a	-559.1538999383	-559.0696783155
^{1}A″-**2′**	-	-384.8106354017
TS(2′ → 3′)	-	-384.7984329120
3′	-384.8823857135	-384.8039036139
TS(3′ → 4′)	-384.8665505346	-384.7945828973
4′	-384.8848588502	-384.8090043445

5. Computational Data

Optimized geometries (Cartesian coordinates, Å), electronic energies (*E*, E_h) and zero-point vibrational energy (ZPVE, E_h) computed at the B3LYP/6-311+G(2d,p), B3LYP/SNSD and CASSCF(8,8)/cc-pVTZ levels of theory.

1s: B3LYP/6-311+G(2d,p) (*E* = -669.733529; ZPVE = 0.090592)

C	-2.208318	-0.371389	-0.000005
C	-1.230131	-1.362169	-0.000006
C	0.099553	-0.985178	0.000000
C	0.523014	0.343697	0.000006
C	-0.502779	1.297570	0.000008
C	-1.842009	0.972171	0.000003
O	-3.542049	-0.653230	-0.000010
H	-3.680472	-1.607201	-0.000014
N	1.845444	0.813845	0.000014
N	2.805240	0.037291	-0.000005
N	3.791030	-0.511664	-0.000018
H	-1.476628	-2.416842	-0.000011
F	1.039822	-1.954547	-0.000001
F	-0.155820	2.593801	0.000015
H	-2.590530	1.752083	0.000004

1a: B3LYP/6-311+G(2d,p) (*E* = -669.733632; ZPVE = 0.090622)

C	-2.201657	-0.403510	-0.000005
C	-1.213286	-1.383571	-0.000004
C	0.108349	-0.991760	0.000002
C	0.521014	0.344510	0.000007
C	-0.510722	1.286344	0.000006
C	-1.849344	0.944146	0.000000
O	-3.497744	-0.825982	-0.000010
H	-4.093873	-0.068430	-0.000011
N	1.839215	0.826059	0.000016
N	2.806093	0.058087	-0.000006
N	3.797145	-0.481097	-0.000022
H	-1.469378	-2.433898	-0.000007
F	1.062582	-1.946338	0.000006
F	-0.183290	2.588465	0.000011
H	-2.591690	1.732738	0.000000

^{3}**2**: B3LYP/6-311+G(2d,p) (*E* = -560.173662; ZPVE = 0.079089)

C	-1.611652	-0.043556	0.000080
C	-0.948869	1.190021	0.000039
C	0.422972	1.207048	-0.000026
C	1.226334	0.025446	-0.000052
C	0.476630	-1.194682	-0.000017
C	-0.890869	-1.244342	0.000049
O	-2.964322	-0.141646	0.000140
H	-3.366145	0.735397	0.000152
N	2.546210	0.056633	-0.000120
H	-1.490993	2.128096	0.000056
F	1.060193	2.384056	-0.000068
F	1.173995	-2.336457	-0.000044
H	-1.406717	-2.194774	0.000077

3s: B3LYP/6-311+G(2d,p) (*E* = -560.145129; ZPVE = 0.079799)

C	1.415117	0.354313	0.029620
C	1.037688	-1.040362	-0.147855
C	-0.250653	-1.437523	-0.079900
C	-1.142661	-0.372838	0.240472
C	-0.881769	1.030429	0.046719
C	0.527698	1.383788	0.119408
O	2.768856	0.514845	0.064725
H	2.986353	1.449031	0.169869
N	-1.640590	0.369985	1.152597
H	1.830617	-1.767393	-0.271817
F	-0.646302	-2.699111	-0.268405
F	-1.639275	1.775222	-0.826632
H	0.853973	2.417870	0.120518

3a: B3LYP/6-311+G(2d,p) (*E* = -560.141810; ZPVE = 0.079367)

C	-1.319728	-0.628465	0.034948
C	-1.212216	0.813414	-0.139938
C	-0.022916	1.453586	-0.073571
C	1.055919	0.581265	0.243337
C	1.064615	-0.849274	0.041994
C	-0.248376	-1.465822	0.108991
O	-2.571237	-1.172916	0.077390
H	-3.244788	-0.485242	0.042933
N	1.671864	-0.061596	1.158908
H	-2.114701	1.400226	-0.276807
F	0.118716	2.766343	-0.277878
F	1.960078	-1.431866	-0.820900
H	-0.386596	-2.538998	0.096826

TS(3a→3s): B3LYP/6-311+G(2d,p) (*E* = -560.138181; ZPVE = 0.078698)

C	-1.399123	-0.403731	0.020159
C	-1.067978	1.003090	-0.149680
C	0.207602	1.446879	-0.075767
C	1.126532	0.412290	0.258479
C	0.919228	-1.004284	0.046190
C	-0.479334	-1.401997	0.087893
O	-2.749347	-0.703005	-0.018636
H	-3.122338	-0.684532	0.870482
N	1.623570	-0.325993	1.173116
H	-1.881599	1.703300	-0.293749
F	0.567997	2.717690	-0.277379
F	1.718631	-1.716287	-0.812509
H	-0.787481	-2.438880	0.045889

TS(3a→3s)': B3LYP/6-311+G(2d,p) (*E* = -560.137643; ZPVE = 0.078712)

C	-1.413398	-0.349231	0.047984
C	-1.027451	1.044253	-0.129378
C	0.265764	1.436947	-0.086249
C	1.150342	0.368179	0.232313
C	0.879379	-1.037954	0.047991
C	-0.533920	-1.380352	0.133270
O	-2.773577	-0.576007	0.161628
H	-3.161999	-0.732605	-0.707181
N	1.645794	-0.378198	1.142941
H	-1.815366	1.781297	-0.225667
F	0.668784	2.695867	-0.280915
F	1.620279	-1.793476	-0.828791
H	-0.880435	-2.405820	0.150994

TS(3s→4s): B3LYP/6-311+G(2d,p) (*E* = -560.131765; ZPVE = 0.077966)

C	-1.064057	-0.975902	0.032203
C	-1.472115	0.366309	0.017164
C	-0.537976	1.392645	0.005843
C	0.690394	1.041024	0.464336
C	1.339071	-0.513240	0.050421
C	0.261554	-1.386035	-0.124391
O	-2.082992	-1.889285	0.063187
H	-1.724134	-2.778828	0.154654
N	1.526660	0.382979	1.147708
H	-2.532472	0.590418	0.004261
F	-0.820109	2.620841	-0.473176
F	2.427229	-0.683614	-0.729039
H	0.468616	-2.362014	-0.551886

4s: B3LYP/6-311+G(2d,p) (*E* = -560.156338; ZPVE = 0.080011)

C	0.288631	1.343384	0.013337
C	1.444824	0.647306	0.257789
C	1.417724	-0.764201	0.042964
C	0.363963	-1.404871	0.513730
C	-1.496560	-0.427636	-0.023515
C	-0.999148	0.798303	-0.347910
O	0.369949	2.698644	0.115598
H	-0.508969	3.093612	0.077492
N	-0.882805	-1.375932	0.752430
H	2.322561	1.174967	0.615502
F	2.421101	-1.384523	-0.617932
F	-2.754814	-0.710849	-0.361274
H	-1.706737	1.478432	-0.810311

4a: B3LYP/6-311+G(2d,p) (*E* = -560.157571; ZPVE = 0.080143)

C	0.345119	1.326420	0.013606
C	1.462447	0.568685	0.264979
C	1.369407	-0.841101	0.049491
C	0.279325	-1.429756	0.501663
C	-1.527056	-0.344827	-0.025630
C	-0.971905	0.857116	-0.337678
O	0.384045	2.684833	0.085352
H	1.289926	2.984708	0.231066
N	-0.961118	-1.333594	0.741902
H	2.373836	1.036062	0.631118
F	2.342374	-1.502372	-0.620010
F	-2.799486	-0.562522	-0.355621
H	-1.638309	1.600536	-0.756222

TS(4s→4a): B3LYP/6-311+G(2d,p) (*E* = -560.149151; ZPVE = 0.078905)

C	0.326104	1.328594	-0.004138
C	1.459350	0.603236	0.231786
C	1.391074	-0.818534	0.053841
C	0.305066	-1.408016	0.511156
C	-1.518748	-0.379193	-0.030821
C	-0.981171	0.828814	-0.354652
O	0.404413	2.711288	0.020431
H	0.338113	3.038897	0.925254
N	-0.930432	-1.330880	0.773758
H	2.370929	1.107829	0.535836
F	2.374878	-1.474609	-0.600618
F	-2.782164	-0.636888	-0.364956
H	-1.655801	1.553198	-0.793714

TS(4s→4a)': B3LYP/6-311+G(2d,p) (*E* = -560.148805; ZPVE = 0.078915)

C	0.338472	1.323150	0.023447
C	1.458013	0.580768	0.272884
C	1.383093	-0.835113	0.052118
C	0.290558	-1.428391	0.484847
C	-1.525080	-0.366226	-0.033543
C	-0.975361	0.844379	-0.331101
O	0.421764	2.695550	0.195100
H	0.597065	3.130922	-0.647681
N	-0.947051	-1.345762	0.738150
H	2.355605	1.071227	0.634715
F	2.367507	-1.477503	-0.616339
F	-2.795979	-0.593990	-0.361542
H	-1.659354	1.585819	-0.725858

1s: B3LYP/SNSD (*E* = -669.563053; ZPVE = 0.091040)

C	2.213765	-0.374333	0.000002
C	1.231458	-1.367174	0.000007
C	-0.101504	-0.986073	0.000005
C	-0.525256	0.347074	-0.000002
C	0.505263	1.301153	-0.000006
C	1.848921	0.974050	-0.000005
O	3.547824	-0.658982	0.000004
H	3.682954	-1.614236	0.000009
N	-1.848371	0.818786	-0.000004
N	-2.807028	0.034843	-0.000001
N	-3.803284	-0.513029	0.000000
H	1.477338	-2.424663	0.000013
F	-1.044639	-1.954716	0.000010
F	0.159298	2.599531	-0.000013
H	2.600091	1.755044	-0.000009

^{3}**2**: B3LYP/SNSD (*E* = -560.034004; ZPVE = 0.079498)

C	-1.617012	-0.044093	0.000075
C	-0.952900	1.193119	0.000038
C	0.423982	1.208489	-0.000027
C	1.230367	0.025645	-0.000059
C	0.478492	-1.195967	-0.000015
C	-0.894239	-1.248169	0.000049
O	-2.970965	-0.142001	0.000140
H	-3.371164	0.736625	0.000154
N	2.555940	0.057404	-0.000120
H	-1.496194	2.133494	0.000058
F	1.061467	2.387667	-0.000063
F	1.176518	-2.339749	-0.000041
H	-1.410501	-2.201350	0.000079

3s: B3LYP/SNSD (*E* = -560.006369; ZPVE = 0.080015)

C	-1.414766	-0.368955	0.029529
C	-1.053377	1.031814	-0.144200
C	0.236543	1.444834	-0.077899
C	1.141885	0.389204	0.240275
C	0.896116	-1.022116	0.047260
C	-0.512476	-1.393179	0.117493
O	-2.767696	-0.547085	0.062679
H	-2.972062	-1.485081	0.167083
N	1.642788	-0.359833	1.154294
H	-1.857037	1.751486	-0.265866
F	0.617804	2.711835	-0.269676
F	1.663955	-1.759289	-0.826768
H	-0.828233	-2.433409	0.110544

4a: B3LYP/SNSD (*E* = -560.016810; ZPVE = 0.080277)

C	0.348173	1.330283	0.015317
C	1.468927	0.566428	0.261346
C	1.367624	-0.844248	0.044245
C	0.275348	-1.439306	0.503395
C	-1.530342	-0.343186	-0.024942
C	-0.971541	0.863811	-0.334904
O	0.392760	2.689781	0.086870
H	1.299741	2.985012	0.240156
N	-0.970874	-1.336289	0.745639
H	2.387297	1.032059	0.620137
F	2.343931	-1.509988	-0.618240
F	-2.804299	-0.556122	-0.360526
H	-1.638824	1.611016	-0.752577

^{1}A"-**2**: CASSCF(8,8)/cc-pVTZ (E=-557.3131157334; ZPVE=0.082895)

N	-0.07805293	-0.95421129	0.30300766
C	-0.10462135	-0.06110994	1.20800960
C	0.94257009	0.08027764	2.22003436
C	0.91560918	1.02960908	3.18318701
C	-1.18568146	0.91547042	1.32841325
C	-1.21714270	1.87033319	2.29359841
C	-0.16808353	1.94358671	3.23646641
H	1.70519233	1.09538090	3.90390420
H	-2.04177141	2.55657220	2.32455564
F	-2.15196514	0.83022094	0.44150713
F	1.93498302	-0.77859491	2.14854765
O	-0.13822268	2.86524677	4.21779156
H	-0.88859618	3.43093729	4.18507814

TS(2→3s): CASSCF(8,8)/cc-pVTZ (E=-557.2958176903; ZPVE=0.083138)

N	0.18680699	-0.00245000	-0.06830007
C	-0.00151827	-0.00441237	1.17469132
C	0.89041013	-0.08134267	2.33695936
C	0.80151004	0.88475788	3.25981855
C	-1.19931710	0.78899795	1.33591688
C	-1.14624429	1.95251787	2.14963293
C	-0.16782099	1.97090292	3.09637618
H	1.46942246	0.92280746	4.09606218
H	-1.89363480	2.71985960	2.08000946
F	-2.32422876	0.46267781	0.75382274
F	1.78184760	-1.03997838	2.39595032
O	0.01012479	2.96882153	3.97603679
H	-0.62796974	3.65050292	3.85769248

3a CASSCF(8,8)/cc-pVTZ (E=-557.3133712354; ZPVE=0.08465)

N	0.28917190	-0.18691537	-0.27148700
C	0.06708919	0.11202268	0.94144785
C	0.63470370	0.00618461	2.26920557
C	1.49755704	0.99354547	2.54908156
C	0.03424222	1.27281952	0.14296862
C	1.14164484	2.20516682	0.38938969
C	1.80312407	2.04541183	1.55543256
H	2.01347971	1.00555968	3.49031305
H	1.37034678	3.01899147	-0.26847419
F	-1.11780405	1.81235683	-0.26012141
F	0.34030885	-0.96991849	3.08941102
O	2.78615499	2.91658163	1.88101852
H	3.39328265	2.54427576	2.49434471

TS(3a→3s): CASSCF(8,8)/cc-pVTZ (E=-557.3116618095; ZPVE=0.084087)

N	-0.01222398	0.54263818	0.06628976
C	0.05670640	-0.01555034	1.20377851
C	0.91680592	-0.17466892	2.35732293
C	0.78791386	0.82357812	3.24378705
C	-1.09270084	0.79538071	1.12503886
C	-1.05918860	1.97303641	2.00572896
C	-0.16216044	1.93371272	3.01300240
H	1.42387772	0.88016927	4.10470676
H	-1.74706697	2.78851724	1.90508258
F	-2.30141234	0.28060868	0.88424993
F	1.76665437	-1.16374958	2.47189021
O	-0.04036412	2.97869420	3.88222337
H	-0.57989019	2.84700346	4.64281893

3s: CASSCF(8,8)/cc-pVTZ (E=-557.3170177567; ZPVE=0.085117)

N	-0.01923295	0.52228433	0.06530289
C	0.05162428	-0.01609785	1.21211958
C	0.91379726	-0.15987955	2.36674666
C	0.78643948	0.84531409	3.24370575
C	-1.09599471	0.79530132	1.12693894
C	-1.05709302	1.98431027	1.98894656
C	-0.15742265	1.95379388	2.99608040
H	1.40842986	0.90829092	4.11368275
H	-1.75791013	2.78933716	1.87440586
F	-2.30569935	0.27827409	0.89535791
F	1.75596344	-1.15290046	2.49787879
O	-0.00465579	2.94104815	3.90280032
H	-0.61470395	3.64071107	3.74915910

TS(3s→4s): CASSCF(8,8)/cc-pVTZ (E=-557.2791207183; ZPVE=0.082933)

N	0.28386357	0.00541881	-0.24431449
C	0.14202280	-0.11984462	1.00616705
C	0.71863389	-0.08015456	2.24375820
C	1.72491920	0.85608548	2.40611124
C	-0.02326079	1.35261226	0.05587316
C	0.93500769	2.25381422	0.52032018
C	1.85650110	1.93057764	1.51847112
H	2.36706901	0.81719333	3.26365376
H	0.85072803	3.27770805	0.20597155
F	-1.15023196	1.81336296	-0.44416466
F	0.25725648	-0.78950328	3.25272584
O	2.87284899	2.78341365	1.80133772
H	3.01025510	3.39363742	1.10039234

4s: CASSCF(8,8)/cc-pVTZ (E=-557.3185958169; ZPVE=0.084995)

N	0.01926215	0.08309273	-0.06613055
C	0.26766476	-0.42877960	1.06142473
C	0.80698276	-0.18761621	2.25294590
C	1.90531003	0.74597025	2.33433676
C	-0.09334650	1.45943987	0.01353359
C	0.70230663	2.27458501	0.73181903
C	1.80249298	1.88865876	1.61895883
H	2.76721668	0.56535161	2.94621634
H	0.57236391	3.32752633	0.56616521
F	-0.98111546	1.97227502	-0.80009234
F	0.33246094	-0.73190856	3.35626364
O	2.79211807	2.80062675	1.75033569
H	2.80163336	3.40728498	1.03246951

TS(4s→4a): CASSCF(8,8)/cc-pVTZ (E=-557.3150612499; ZPVE=0.084082)

N	-0.02161364	0.07647306	-0.05494003
C	0.22899498	-0.43548033	1.07068610
C	0.80150807	-0.21341173	2.24855185
C	1.89948881	0.72591990	2.31915665
C	-0.12627319	1.45710695	0.02460830
C	0.69679248	2.26278329	0.72143865
C	1.80074787	1.86433768	1.59823358
H	2.75191498	0.55019701	2.94685698
H	0.61220586	3.31595063	0.54137850
F	-1.01692855	1.97138429	-0.78548396
F	0.35149005	-0.75878757	3.36189628
O	2.77728915	2.81514287	1.69595647
H	3.53432870	2.57509303	1.19036460

4a: CASSCF(8,8)/cc-pVTZ (E=-557.3201845687; ZPVE=0.085237)

N	-0.03200223	0.07728115	-0.05106344
C	0.22769929	-0.44082871	1.06986272
C	0.80565417	-0.21657120	2.24497914
C	1.91186333	0.70989627	2.30725789
C	-0.11875001	1.45740771	0.02862367
C	0.70336390	2.26113701	0.72774792
C	1.80743051	1.85872388	1.59975719
H	2.77787709	0.50255769	2.90929699
H	0.62581569	3.31369972	0.54258829
F	-1.00540149	1.98091936	-0.77963310
F	0.35074863	-0.75220907	3.36218739
O	2.76078534	2.81258154	1.63133740
H	3.43952918	2.59858084	2.24670291

3': B3LYP/6-311+G(2d,p) (*E* = -385.621481; ZPVE = 0.083466)

C	0.851298	1.498444	-0.177643
C	-0.585045	1.290955	-0.117322
C	-1.101840	0.055567	0.042062
C	-0.104651	-0.973445	0.049654
C	1.300837	-0.801829	0.452437
C	1.767643	0.539358	0.123990
N	0.632700	-1.695335	-0.667145
H	-1.253225	2.136490	-0.227800
F	-2.409089	-0.207335	0.173267
H	2.813121	0.805323	0.235194
H	1.737070	-1.366380	1.266891
H	1.186483	2.503642	-0.402736

TS(3'→4'): B3LYP/6-311+G(2d,p) (*E* = -385.610075; ZPVE = 0.081778)

C	0.728872	1.513051	-0.201461
C	-0.643185	1.233212	-0.268334
C	-1.130223	-0.044449	-0.037045
C	-0.180139	-1.019472	-0.157342
C	1.482480	-0.761365	0.415075
C	1.677172	0.611616	0.295038
N	0.820674	-1.540433	-0.674046
H	-1.351683	2.036253	-0.440621
F	-2.394819	-0.294866	0.365363
H	2.564008	1.023810	0.768059
H	1.034953	2.539304	-0.361542
H	1.951510	-1.358095	1.188578

4': B3LYP/6-311+G(2d,p) (*E* = -385.630229; ZPVE = 0.083584)

C	0.560130	1.522957	-0.134380
C	-0.727738	1.187730	-0.409340
C	-1.168197	-0.150628	-0.083590
C	-0.289249	-1.095225	-0.336695
C	1.760042	-0.668904	0.286683
C	1.597650	0.674084	0.422313
N	0.901831	-1.445640	-0.514510
H	-1.404491	1.906830	-0.862865
F	-2.358550	-0.353491	0.528513
H	2.418982	1.197579	0.900846
H	0.864764	2.544852	-0.340765
H	2.639049	-1.168443	0.677797

^{1}A"-**2'**: CASSCF(8,8)/cc-pVTZ (E=-383.5422261284; ZPVE=0086108)

N	-0.01760804	-0.83889145	0.24078618
C	-0.11205294	-0.01685311	1.20485950
C	0.90793008	0.07362051	2.25326157
C	0.81610024	0.94600564	3.28424668
C	-1.25152099	0.90156025	1.33648264
C	-1.32228720	1.77054965	2.38249660
C	-0.30412790	1.81709552	3.37314510
H	1.59211648	0.96917003	4.02350235
H	-2.16068006	2.43465424	2.46455073
F	1.93391168	-0.74381471	2.14675951
H	-0.37617496	2.50664663	4.18859243
H	-2.01207614	0.85694039	0.58392841

TS(2'→3'): CASSCF(8,8)/cc-pVTZ (E=-383.5281307427; ZPVE=0.085940)

N	0.20420659	0.11507051	-0.06555077
C	0.01481714	0.02059585	1.17050743
C	0.88449013	-0.08143432	2.34275055
C	0.78481919	0.88635486	3.26306915
C	-1.21045542	0.79096359	1.26970720
C	-1.13566267	1.95210469	2.11156535
C	-0.18057960	1.97590423	3.08208418
H	1.44303286	0.89396477	4.10921955
H	-1.87123954	2.73030257	2.04900193
F	1.76609588	-1.05410779	2.40733027
H	-0.13440271	2.79467273	3.77272749
H	-2.05972481	0.52814633	0.68180847

3': CASSCF(8,8)/cc-pVTZ (E=-383.5355428704; ZPVE=0.087813)

N	0.00358762	0.45578957	0.06536839
C	0.05370629	-0.03985459	1.21629882
C	0.93646640	-0.13410291	2.36655307
C	0.81061178	0.88495535	3.22651196
C	-1.17422414	0.69659144	1.16337466
C	-1.11286247	1.90512002	2.00631213
C	-0.16529971	1.96092331	2.97012639
H	1.44897604	0.94695055	4.08582878
H	-1.84092498	2.68823624	1.91339016
F	1.79259193	-1.12067890	2.49904060
H	-0.11432767	2.81445765	3.61824679
H	-2.10796547	0.23653908	0.91249138

TS(3'→4'): CASSCF(8,8)/cc-pVTZ (E=-383.5006782972; ZPVE=0.086226)

N	0.63729614	-0.08385323	-0.26691648
C	0.30175108	-0.17348327	0.93202764
C	0.73702443	-0.10020342	2.23291254
C	1.66134560	0.89548904	2.48422813
C	0.16534744	1.28764927	-0.09915451
C	1.03183889	2.21800470	0.48390180
C	1.85439074	1.95459998	1.58185053
H	2.15765929	0.91381550	3.43552136
H	0.95213157	3.23872924	0.15723279
F	0.18522750	-0.81602520	3.19539666
H	2.55229139	2.71622658	1.87149644
H	-0.72323543	1.56565750	-0.62985033

4': CASSCF(8,8)/cc-pVTZ (E=-383.537097608; ZPVE=0.087999)

N	0.49204755	-0.00768875	-0.22899680
C	0.47170976	-0.44875714	0.94787818
C	0.77184737	-0.16770425	2.20821452
C	1.78373587	0.84668303	2.45373368
C	0.26417568	1.38329411	-0.28195888
C	0.88199216	2.24469328	0.55528128
C	1.79546177	1.94381833	1.66535628
H	2.48925877	0.73168206	3.25530267
H	0.76034218	3.28891659	0.33446485
F	0.12779401	-0.69630444	3.23494792
H	2.52753162	2.70331192	1.87054884
H	-0.32479480	1.73636019	-1.10475194

6. References

S1 K. Kanakarajan, K. Haider and A. W. Czarnik, *Synthesis*, 1988, 566–568.

S2 A. D. Becke, *J. Chem. Phys.*, 1993, **98**, 5648–5652.

S3 A. D. Becke, *Phys. Rev. A*, 1988, **38**, 3098–3100.

S4 C. Lee, W. Yang and R. G. Parr, *Phys. Rev. B*, 1988, **37**, 785–789.

S5 S. H. Vosko, L. Wilk and M. Nusair, *Can. J. Phys.*, 1980, **58**, 1200–1211.

S6 M. J. Frisch, G. W. Trucks, H. B. Schlegel, G. E. Scuseria, M. A. Robb, J. R. Cheeseman, G. Scalmani, V. Barone, G. A. Petersson, H. Nakatsuji, X. Li, M. Caricato, A. V. Marenich, J. Bloino, B. G. Janesko, R. Gomperts, B. Mennucci, H. P. Hratchian, J. V. Ortiz, A. F. Izmaylov, J. L. Sonnenberg, D. Williams-Young, F. Ding, F. Lipparini, F. Egidi, J. Goings, B. Peng, A. Petrone, T. Henderson, D. Ranasinghe, V. G. Zakrzewski, J. Gao, N. Rega, G. Zheng, W. Liang, M. Hada, M. Ehara, K. Toyota, R. Fukuda, J. Hasegawa, M. Ishida, T. Nakajima, Y. Honda, O. Kitao, H. Nakai, T. Vreven, K. Throssell, J. A. Montgomery, Jr., J. E. Peralta, F. Ogliaro, M. J. Bearpark, J. J. Heyd, E. N. Brothers, K. N. Kudin, V. N. Staroverov, T. A. Keith, R. Kobayashi, J. Normand, K. Raghavachari, A. P. Rendell, J. C. Burant, S. S. Iyengar, J. Tomasi, M. Cossi, J. M. Millam, M. Klene, C. Adamo, R. Cammi, J. W. Ochterski, R. L. Martin, K. Morokuma, O. Farkas, J. B. Foresman, and D. J. Fox, *Gaussian 16, Revision B.01*. 2016.

S7 C. M. Nunes, A. K. Eckhardt, I. Reva, R. Fausto, P. R. Schreiner, *J. Am. Chem. Soc.*, 2019, **141**, 14340–14348.

S8 V. Barone, *J. Chem. Phys.*, 2005, **122**, 014108.

S9 J. Bloino, V. Barone, *J. Chem. Phys.*, 2012, **136**, 124108.

S10 Double and triple-ζ basis sets of SNS, are available for download at https://smart.sns.it (accessed July 1, 2021).

S11 T. H. Dunning, *J. Chem. Phys.*, 1989, **90**, 1007–1023.

S12 P. Piecuch, S. A. Kucharski, K. Kowalski and M. Musiał, *Comput. Phys. Commun.*, 2002, **149**, 71–96.

S13 J. L. Bentz, R. M. Olson, M. S. Gordon, M. W. Schmidt and R. A. Kendall, *Comput.*

Phys. Commun., 2007, **176**, 589–600.

S14 R. M. Olson, J. L. Bentz, R. A. Kendall, M. W. Schmidt and M. S. Gordon, *J. Chem. Theory Comput.*, 2007, **3**, 1312–1328.

S15 M. W. Schmidt, K. K. Baldridge, J. A. Boatz, S. T. Elbert, M. S. Gordon, J. H. Jensen, S. Koseki, N. Matsunaga, K. A. Nguyen, S. Su, T. L. Windus, M. Dupuis and J. A. Montgomery, *J. Comput. Chem.*, 1993, **14**, 1347–1363.

S16 P. E. M. Siegbahn, J. Almlöf, A. Heiberg and B. O. Roos, *J. Chem. Phys.*, 1981, **74**, 2384–2396.

S17 K. Ruedenberg, M. W. Schmidt, M. M. Gilbert and S. T. Elbert, *Chem. Phys.*, 1982, **71**, 65–78.

S18 B. O. Roos, P. R. Taylor and P. E. M. Sigbahn, *Chem. Phys.*, 1980, **48**, 157–173.

S19 P. Siegbahn, A. Heiberg, B. Roos and B. Levy, *Phys. Scr.*, 1980, **21**, 323–327.

S20 N. P. Gritsan, A. D. Gudmundsdóttir, D. Tigelaar, Z. Zhu, W. L. Karney, C. M. Hadad and M. S. Platz, *J. Am. Chem. Soc.*, 2001, **123**, 1951–1962.

S21 W. L. Karney and W. T. Borden, *J. Am. Chem. Soc.*, 1997, **119**, 1378–1387.

S22 K. Hirao, *Chem. Phys. Lett.*, 1993, **201**, 59–66.

S23 K. Hirao, *Int. J. Quantum Chem.*, 1992, **44**, 517–526.

S24 K. Hirao, *Chem. Phys. Lett.*, 1992, **196**, 397–403.

S25 K. Hirao, *Chem. Phys. Lett.*, 1992, **190**, 374–380.

S26 C. M. Nunes, I. Reva, R. Fausto, In *Tunnelling in Molecules: Nuclear Quantum Effects from Bio to Physical Chemistry*; S. Kozuch, J. Kästner, Eds.; Royal Society of Chemistry, 2021; pp 1–60.

S27 L. Brillouin, *Compt. Rend. Hebd. Seances Acad. Sci.*, 1926, **183**, 24–26.

S28 G. Wentzel, *Zeitschrift für Phys.*, 1926, **38**, 518–529.

S29 H. A. Kramers, *Zeitschrift für Phys.*, 1926, **39**, 828–840.

S30 W. T. Borden,*WIREs Comput. Mol. Sci.*, 2016, **6**, 20–46.

S31 G. A. Zhurko, *ChemCraft*, *Version 1.8*. http://www.chemcraftprog.com, 2016.